

# Symmetry-driven Phononic Metamaterials

Simon Yves<sup>1</sup>, Romain Fleury<sup>2</sup>, Gal Shmuel<sup>3</sup>, Michel Fruchart<sup>4</sup>, Vincenzo Vitelli<sup>5,6</sup>, Michael R. Haberman<sup>7,\*</sup>, and Andrea Alù<sup>1,8,\*</sup>

<sup>1</sup>Photonics Initiative, Advanced Science Research Center, City University of New York, New York, NY 10031, USA

<sup>2</sup>Laboratory of Wave Engineering, EPFL, 1015 Lausanne, Switzerland

<sup>3</sup>Faculty of Mechanical Engineering, Technion–Israel Institute of Technology, Haifa 32000, Israel

<sup>4</sup>ESPCI, Laboratoire Gulliver, 10 rue Vauquelin, 75231 Paris cedex 05

<sup>5</sup>University of Chicago, James Franck Institute, 929 E 57th Street, Chicago, IL 60637

<sup>6</sup>University of Chicago, Kadanoff Center for Theoretical Physics, 933 E 56th St, Chicago, IL 60637

<sup>7</sup>Walker Department of Mechanical Engineering, The University of Texas at Austin, Austin, Texas 78712, USA

<sup>8</sup>Physics Program, Graduate Center, City University of New York, New York, NY 10026, USA

\*Corresponding authors: aalu@gc.cuny.edu; haberman@utexas.edu

## ABSTRACT

Phonons are quasi-particles associated with mechanical vibrations in materials, at the root of the propagation of sound, elastic / mechanical waves, and of thermal phenomena, common to our every day life and many technologies. The fundamental understanding and control over phonon responses in natural and artificial media is of major importance in the context of telecommunications, shielding, energy harvesting and control, sensing and imaging, across multiple scales. In this context, it has been recently realized that controlling different classes of symmetries at the microscopic and mesoscopic scale offers a powerful rational tool to precisely tailor phononic responses, leading to advanced acoustic and elastodynamic wave control. In this paper, we review the recent advances in the design and synthesis of artificial phononic media, namely phononic metamaterials, guided by symmetry principles. Starting from tailored broken spatial symmetries, we discuss their interplay with time symmetries for non-reciprocity and non-conservative phenomena, and finally address broader concepts that combine multiple symmetry classes to support exotic phononic wave transport.

## 1 Introduction

Symmetries play a fundamental role in the general understanding of several phenomena in nature. Physicists and engineers have been hunting for the presence or absence of symmetries in systems to not only understand, but also tailor their physical properties. This paradigm has recently flourished in the context of acoustic and elastic wave propagation, realizing how various classes of symmetries may describe and enable unprecedented control over phonon fields. The thorough investigation of these symmetries permits the definition of the bounds inherent to wave properties, and how their purposeful breaking can result in enhanced manipulation of acoustic and elastic waves. In this context, artificial phononic crystals and metamaterials<sup>1–6</sup>, which have been extensively studied for over two decades, have become a successful platform to implement symmetry-driven acoustic and elastodynamic manipulation. In this paper, we review recent advances in the field of phononic meta-structures from the perspective of their underlying symmetries (Fig. 1). The broad definition of phonons, namely modes of mechanical vibrations, spans a large collection of domains in physics, both quantum and classical, whose denominations are not always clearly defined. Here, we focus mainly on elastic waves in solids (elastodynamics) and sound in gases and liquids (acoustics), and how engineering the symmetries of artificial media supporting their propagation allows for their tailored control. While we are used to think of symmetry as spatial mapping between two sides of an object, the concept of symmetry is very general: any transformation that keeps an object unchanged corresponds to a symmetry class. Here, we focus on the most relevant ones for the general control of phononic waves. Starting from basic spatial symmetries, we combine them with temporal transformations, with implications in reciprocity and energy conservation. We then discuss broader concepts that extend metamaterial design beyond strict symmetry-engineering.

We first focus on spatial symmetries at scales spanning from the individual meta-atom forming the metamaterial to the entire medium. This allows for a review of the latest advances related to Willis and electro-momentum coupling metamaterials, as well as anisotropic and hyperbolic metasurfaces, nonlocal properties and angular momentum engineering. If spatial symmetry engineering may appear to be the most straightforward in the context of symmetry-driven phononic metamaterials, it is fundamentally limited to the degree of control over phonon fields, since any arbitrarily complex spatial pattern still obeys time-reversal symmetry and reciprocity. In order to break the inherent symmetry in wave propagation between two ports, one needs to either introduce nonlinearities into the picture, or engineer temporal symmetries. In the second section, we review

recent works related to broken reciprocity using nonlinearity, time-reversal symmetry breaking and time-varying media. In particular, we discuss the recent demonstrations of odd Willis coupling, odd viscosity, and non-reciprocal phononic metasurfaces from a unified perspective.

Next, we go beyond quasi-conservative spatial and temporal symmetries and focus on the engineering of the energy balance within artificial phononic media. Through the study of parity-time ( $\mathcal{PT}$ ) symmetry, we present scenarios where gain and loss are purposely added to the system, providing an additional degree of freedom to manipulate wave motion. We also examine how these non-Hermitian features permit the control of wave dynamics within open scattering systems, and connect this area of research with recent approaches, such as complex frequency excitations. Besides, we present non-Hermitian responses specific to elastodynamic waves, such as odd elasticity and exceptional points in conservative solids.

In the final section, we go beyond symmetry engineering of the underlying phononic materials and focus on concepts that connect symmetries and phononics within a global perspective. Based on topological concepts, we show how the unit cell symmetries within the bulk of a medium determine the wave behavior at its boundaries, and review recent developments of the emerging role of dualities in phononic metamaterial design. Finally, we showcase how the rotation degree of freedom in multilayer systems brings new opportunities for global manipulation of symmetries in the context of twistronics for phonons.

The goal of this review is to present from a unified rational perspective the latest advances in the field of artificial phononic media under the paradigm of multiscale symmetries and symmetry breaking. While several reviews related to acoustic and elastic metamaterials and metasurfaces have appeared in the recent literature<sup>1,3-6</sup>, the articulation of these recent advances around different classes of symmetry-engineering provides a powerful perspective for phononic metamaterials, and provides insights into the creation of new meta-structures for phonon control.

## 2 Spatial symmetry

Phononic wave phenomena include mechanical waves, such as longitudinal acoustic waves propagating in fluids and gases<sup>7</sup>, and longitudinal and transverse waves in elastic solids<sup>8</sup>. In linear elasticity, the stress  $\boldsymbol{\sigma}$  is commonly assumed to be related to strain via Hooke's law, as described by the Cauchy momentum equation  $\nabla \cdot \boldsymbol{\sigma} + \mathbf{F} = \rho \ddot{\mathbf{u}}$ , in which the displacement field  $\mathbf{u}$  is the variable that describes wave motion,  $\mathbf{F}$  accounts for the body forces and  $\rho$  is the material mass density. In fluids or gasses, the variable describing wave propagation is the pressure  $p$ , whose isentropic variations are related to changes in density via thermodynamic relations, thereby making it natural to describe the associated wave propagation in terms of volume strain, dependent on the pressure via the compressibility  $\beta = \rho_0^{-1} \partial \rho / \partial p|_{s=0}$ . Overall, acoustic (elastic) fields, such as pressure (stress) and particle velocity (displacement), obey intrinsic spatial symmetries that are the consequence of conservation of energy, as well as linear and angular momentum. Consequently, their interaction with a medium is governed by the complementarity between the underlying spatial symmetries at length scales that are much smaller than the wavelength of propagating waves, which is defined as the microscopic scale. This puts spatial symmetry-engineering of elementary inclusions at the core of phononic wave manipulation. In this section, we review macroscopically-observable, dynamic effective behaviors of acoustic and elastic waves that emerge due to broken symmetries at the scale of elementary scatterers that make up an artificial medium. These features include Willis coupling, electro-momentum coupling, media with anisotropic dynamic density, hyperbolic dispersion, nonlocal effects, and orbital angular momentum.

We start with effects that can be captured through continuum theory with fields such as the density  $\rho(\mathbf{r}, t)$  or the displacement  $\mathbf{u}(\mathbf{r}, t)$ . In some cases, it is also useful to consider a discrete description, where the degrees of freedom are associated with discrete resonators, for instance the displacements of atoms in a classical description of an elastic solid, or the meta-atoms in Fig. 1.

### 2.1 Willis coupling

The elastodynamic response of materials is commonly captured by constitutive relations, which describe the relation between physical quantities through material properties such as the medium stiffness and mass density. In conventional elastic media, under the assumptions of locality and linearity, the stress  $\boldsymbol{\sigma}$  tensor is (tensorially) proportional to the gradient of the displacement field  $\nabla \mathbf{u}$  through the elasticity tensor  $\mathbf{C}$  (Hooke's law), and the linear momentum density  $\boldsymbol{\mu}$  to the velocity field  $\dot{\mathbf{u}}$  through the mass density  $\rho$ . Thus, at each point in space  $\mathbf{r}$ , the constitutive relations are  $\boldsymbol{\sigma}(\mathbf{r}) = \mathbf{C}(\mathbf{r}) : \nabla \mathbf{u}(\mathbf{r})$  and  $\boldsymbol{\mu}(\mathbf{r}) = \rho(\mathbf{r}) \dot{\mathbf{u}}(\mathbf{r})$ , with the corresponding components  $\sigma_{ij}(\mathbf{r}) = C_{ijkl}(\mathbf{r})(\partial_{k,l} u(\mathbf{r}) + \partial_{l,k} u(\mathbf{r}))/2$  and  $\mu_i(\mathbf{r}) = \rho_{ij}(\mathbf{r}) \dot{u}_j$ , respectively. Willis was the first to notice that weak forms of nonlocality arising in the material response of heterogeneous random elastic media<sup>9,10</sup> may lead to coupled effective constitutive relations, which relate stress to velocity and momentum to strain. The corresponding coupling tensors,  $\tilde{\mathbf{S}}$  and  $\tilde{\mathbf{S}}^\dagger$ , are known as Willis coupling tensors. In symbolic matrix notation, the generalized coupled constitutive relations are given by

$$\begin{pmatrix} \langle \boldsymbol{\sigma} \rangle \\ \langle \boldsymbol{\mu} \rangle \end{pmatrix} = \begin{pmatrix} \tilde{\mathbf{C}} & \tilde{\mathbf{S}} \\ \tilde{\mathbf{S}}^\dagger & \tilde{\boldsymbol{\rho}} \end{pmatrix} \begin{pmatrix} \langle \nabla \mathbf{u} \rangle \\ \langle \dot{\mathbf{u}} \rangle \end{pmatrix}, \quad (1)$$

where  $\langle \cdot \rangle$  denotes the effective fields obtained by ensemble averaging over the entire medium, and the matrix elements represent nonlocal operators in time and space, such that, e.g.,  $\{\tilde{\mathbf{C}} : \langle \nabla \mathbf{u} \rangle\}(\mathbf{r}, t) = \int_{-\infty}^t \int_{\Omega} \tilde{\mathbf{C}}(\mathbf{r}, \boldsymbol{\chi}, t - \tau) : \langle \nabla \mathbf{u} \rangle(\boldsymbol{\chi}, \tau) d\tau d\boldsymbol{\chi}$ , where  $\Omega$  is the volume of the body. Willis coupling is typically negligible in natural materials, but it may be found and largely enhanced in metamaterials<sup>11</sup>. When the materials involved are reciprocal, the constitutive operator is necessarily self-adjoint<sup>10,12</sup>, such that  $\mathbf{S}^\dagger$  is the adjoint operator of  $\mathbf{S}$  in the sense  $\int_{\Omega} \tilde{\mathbf{S}}(\dot{\mathbf{u}}(\boldsymbol{\chi})) : \nabla \mathbf{u}(\mathbf{r}) d\mathbf{r} = \int_{\Omega} \dot{\mathbf{u}}(\mathbf{r}) \cdot \tilde{\mathbf{S}}^\dagger(\nabla \mathbf{u}(\boldsymbol{\chi})) d\mathbf{r}$ . If the microstructure is sufficiently small relative to the wavelength, the resultant equations become spatially local such that the constitutive response at any material point depends only on the fields at that point. This form of constitutive relations have been referred to as the Milton-Briane-Willis equations<sup>13,14</sup>. In this case, Willis coupling originates from spatial asymmetry in the elastic impedance<sup>15-17</sup> (BOX1), as in the case of an elastic structured beam made of resonant meta-atoms with broken spatial inversion symmetry<sup>17</sup>, which results in a nonzero Willis coupling element relating momentum ( $P_z$ ) and strain ( $\partial_x u_z$ ) (Fig. 2a). These coupling elements are even, purely imaginary functions of the wavevector in lossless media<sup>15,18,19</sup> and obey the relation  $S_{ijk}^\dagger = S_{jki} = -S_{jki}^*$  in reciprocal passive media<sup>18</sup>. Willis coupling tensors are the phononic analogue of bianisotropic tensors in electromagnetism<sup>13,15,20</sup>, which couple the electric and magnetic displacement vectors to both the electric and magnetic fields because of magnetoelectric coupling<sup>21</sup>.

Willis couplings exist also in the absence of rotational fields<sup>22</sup>, hence it can also emerge in fluid acoustics and for longitudinal sound<sup>11,15,23-26</sup>. In such a scenario, the coupled constitutive relations can be written as a function of the acoustic particle velocity  $\mathbf{v}$  (vector field) and the acoustic pressure  $p$  (scalar field). The constitutive relations in this form reflect the coupling between the conservation of mass ( $\nabla \cdot \mathbf{v} = -\beta \dot{p}$ ) and of momentum ( $\nabla p = -\rho \dot{\mathbf{v}}$ ) via the acoustic Willis coupling coefficients  $\boldsymbol{\zeta}$  and  $\boldsymbol{\xi}$ <sup>15,25</sup>, as experimentally demonstrated using a subwavelength asymmetric scatterer in a one-dimensional impedance tube measurement (Fig. 2b)<sup>27</sup>. In the frequency domain:

$$\begin{pmatrix} \nabla \cdot \mathbf{v} \\ \nabla p \end{pmatrix} = i\omega \begin{pmatrix} \beta & \boldsymbol{\xi} \\ \boldsymbol{\zeta} & \boldsymbol{\rho} \end{pmatrix} \begin{pmatrix} p \\ \mathbf{v} \end{pmatrix}, \quad (2)$$

where  $\omega$  is the radian frequency in the  $e^{-i\omega t}$  time convention,  $\beta$  is the scalar compressibility and  $\boldsymbol{\rho}$  is the dynamic acoustic mass density tensor. This framework provides insights into the physical mechanisms behind Willis coupling, and highlights the relevance of spatial symmetry-breaking<sup>11,28</sup>.

We can appreciate this by considering the response to an impinging sound wave for a subwavelength acoustic scatterer of relevant linear dimension  $a$ , with  $ka \ll 1$ , where  $k$  is the wavenumber. Its scattering is dominated by monopole  $M_A$  and dipole  $\mathbf{D}_A$  fields, which are spatially symmetric and anti-symmetric, respectively. They are related to the local pressure  $p$  and particle velocity  $\mathbf{v}$  field at the scatterer position via the effective polarizability tensor  $\tilde{\boldsymbol{\alpha}}$  such as<sup>11</sup>

$$\begin{pmatrix} M_A \\ \mathbf{D}_A \end{pmatrix} = \tilde{\boldsymbol{\alpha}} \begin{pmatrix} p \\ \mathbf{v} \end{pmatrix} = \begin{pmatrix} \tilde{\alpha}_{pp} & \tilde{\boldsymbol{\alpha}}_{pv} \\ \tilde{\boldsymbol{\alpha}}_{vp} & \tilde{\boldsymbol{\alpha}}_{vv} \end{pmatrix} \begin{pmatrix} p \\ \mathbf{v} \end{pmatrix}, \quad (3)$$

If the scatterer is mirror-symmetric with respect to  $\mathbf{v}$ , the polarizability tensor is diagonal, because the spatial symmetry requires that the scalar pressure only excites the monopole, with an isotropic radiation pattern, while the particle velocity excites a dipole moment polarized in the same direction. However, if the scatterer symmetry is broken with respect to the direction of incidence, the  $p$  and  $\mathbf{v}$  fields both contribute to monopolar *and* dipolar scattered fields, leading to non-zero off-diagonal components of the polarizability tensor. These are the scattering analogues of the Willis coupling coefficients. Due to time-reversal symmetry and absence of dissipation,  $\tilde{\boldsymbol{\alpha}}_{vp} = -\tilde{\boldsymbol{\alpha}}_{pv}^T$ , after proper normalization of the polarization tensor so that all its components share the same units<sup>11</sup>. This ensures that the forward scattering is equal for waves impinging from opposite directions, because of reciprocity<sup>29</sup>, while the backward scattering can be drastically different for nonzero  $\boldsymbol{\alpha}_{vp}$ . The constraints associated with time-reversal, linearity and energy conservation yield theoretical bounds for the off-diagonal elements of (3)<sup>11</sup>. Maximum coupling elements emerge at resonance in strongly asymmetric resonators, such as a metallic split ring (Helmholtz resonator), as shown in Fig. 2c, yielding off-diagonal polarizability tensors of the same magnitude as the diagonal ones. An array of such asymmetric scatterers (from the acoustic perspective), all oriented in the same direction, results in the homogeneous limit into macroscopic acoustic Willis coupling  $\boldsymbol{\xi}$  and  $\boldsymbol{\zeta}$ <sup>15</sup>, forming metamaterials with largely asymmetric acoustic response. Overall, these concepts enable expanding the toolset of designer matter for phononic technologies, enabling Willis metamaterials for sound<sup>26,30-32</sup> and elastic waves<sup>17,33,34</sup>, permitting wavefront and particle manipulation<sup>35</sup>.

## 2.2 Electromomentum coupling

In a similar fashion, it is possible to design phononic metamaterials with cross-couplings different from acoustic and elastodynamic Willis couplings by harnessing additional asymmetries provided by piezoelectric constituents. The piezoelectric effect describes the change in electric polarization in certain solids when they are mechanically strained. In turn, the inverse piezoelectric effect corresponds to the generation of stress in response to an electric field. The origin of this electromechanical

coupling is a crystalline structure with broken spatial symmetry<sup>36</sup>. Accordingly, the stress in a piezoelectric material is related to the gradient of the displacement field and the gradient of the electric potential field via the relation  $\boldsymbol{\sigma} = \mathbf{C} : \nabla \mathbf{u} + \mathbf{B}^T \cdot \nabla \phi$ , where  $\mathbf{B}$  is the piezoelectric coupling tensor in stress-charge form and  $\phi$  is the electric potential. Similarly, the electric displacement field  $\mathbf{D}$  in a piezoelectric medium is also a function of the same fields through the relation  $\mathbf{D} = \mathbf{B} \cdot \nabla \mathbf{u} - \mathbf{A} \cdot \nabla \phi$  where  $\mathbf{A}$  is the dielectric permittivity tensor. While the local Willis effect and the piezoelectric effect are seemingly unrelated phenomena, they both describe a form of coupling between physical fields as the result of spatial-symmetry breaking at the microscale (BOX1). In Willis materials, it is the coupling of dynamics and elasticity by breaking elastic impedance symmetry; in piezoelectricity, it is the coupling of electrostatics and elasticity by breaking centrosymmetry in the atomic structure. Shmuel and collaborators<sup>16, 19, 37–40</sup> showed that the combination of these broken atomic and mesoscale symmetries leads to an emergent constitutive coupling between electrostatics and dynamics, such that the electric polarization and velocity fields are coupled as are the linear momentum and the electric field, by the so-called electromomentum couplings<sup>37</sup> (Fig. 2d). As a result, each one of the kinetic fields (stress, linear momentum density, electric displacement) depends on all three kinematic fields (strain, velocity, electric field) (BOX1). In symbolic matrix notation, the constitutive relations of electromomentum-coupled materials take the form

$$\begin{pmatrix} \langle \boldsymbol{\sigma} \rangle \\ \langle \mathbf{D} \rangle \\ \langle \boldsymbol{\mu} \rangle \end{pmatrix} = \begin{pmatrix} \tilde{\mathbf{C}} & \tilde{\mathbf{B}}^\dagger & \tilde{\mathbf{S}} \\ \tilde{\mathbf{B}} & -\tilde{\mathbf{A}} & \tilde{\mathbf{W}} \\ \tilde{\mathbf{S}}^\dagger & \tilde{\mathbf{W}}^\dagger & \tilde{\boldsymbol{\rho}} \end{pmatrix} \begin{pmatrix} \langle \nabla \mathbf{u} \rangle \\ \langle \nabla \phi \rangle \\ \langle \dot{\mathbf{u}} \rangle \end{pmatrix}, \quad (4)$$

where  $\tilde{\mathbf{W}}^\dagger$  and  $\tilde{\mathbf{W}}$  are the electromomentum coupling tensors. Analogous to the Willis coupling tensors, the electromomentum coupling tensors are due to local and nonlocal effects, with their local part depending on spatial symmetry breaking of some material properties<sup>16, 40</sup>. If the constituents are reciprocal, then the constitutive operator is self-adjoint,  $\tilde{\mathbf{W}}^\dagger$  and  $\tilde{\mathbf{W}}$  satisfy<sup>19</sup>  $\int_{\Omega} \tilde{\mathbf{W}}(\dot{\mathbf{u}}(\boldsymbol{\chi})) \cdot \nabla \phi(\mathbf{r}) \, d\mathbf{r} = \int_{\Omega} \dot{\mathbf{u}}(\mathbf{r}) \cdot \tilde{\mathbf{W}}^\dagger(\nabla \phi(\boldsymbol{\chi})) \, d\mathbf{r}$ . In the local limit, the electromomentum tensors are imaginary even functions of the wavevector owing to reciprocity<sup>19, 37</sup> and satisfy  $W_{ij}^\dagger = W_{ji} = -W_{ji}^*$ . Distinct from the Willis effect, the electromomentum effect depends on the circuit conditions, hence it can be exploited as an electrically tunable degree of freedom for wave manipulation<sup>16, 41, 42</sup>, and scattering<sup>43, 44</sup>. This functionality originates from the impact it has on plane waves: it alters the phase velocity similar to the piezoelectric effect, and it generates asymmetry in the phase angle similar to the Willis effect<sup>16, 42</sup>. Recent works analyzing the polarizability of electromomentum-coupled scatterers<sup>43, 45</sup> have shown that the polarizability tensor must consider both electric and magnetic field scattering, due to the time-varying nature of all fields, and that the polarizabilities coupling mechanical and electric fields can reach the same magnitude as the diagonal terms, even when the Willis coefficients vanish<sup>16</sup>.

## 2.3 Spatial anisotropy

### Anisotropy engineering

The role of spatial symmetries becomes even more important for the control of phononic waves as the dimensionality of the medium increases. In this context, anisotropic meta-structures can offer powerful opportunities for acoustic and elastic wave manipulation<sup>3, 4, 46</sup>. The interaction of such structures with an impinging wave is described using effective constitutive tensors whose entries describe the material response along the different directions of space. As an example, consider a 2D collection of subwavelength resonators consisting of circular cavities carved in a rigid medium, which individually host a mass connected to the boundary by springs<sup>47</sup> (Fig. 2e, top panel). The system's effective macroscopic response can be described by a second-order dynamic mass density tensor  $\tilde{\boldsymbol{\rho}}$  of the form

$$\tilde{\boldsymbol{\rho}} = \begin{pmatrix} \rho_{xx} & \rho_{xy} \\ \rho_{yx} & \rho_{yy} \end{pmatrix}. \quad (5)$$

In the absence of material loss, these elements are real-valued and, due to the resonant and directional nature of the elementary constituents, they can be either positive or negative, corresponding to an in-phase or out-of-phase macroscopic response of the medium, respectively<sup>47</sup>. In the case of a diagonal mass density tensor, the resulting dispersion relation in the  $(k_x, k_y)$  plane can be written as  $k_x/\rho_{xx} + k_y/\rho_{yy} = \beta\omega^2$ , where  $\beta$  is the scalar compressibility. This relation shows that the tensor components dictate the shape of the isofrequency contours of the system, which describes the spatial properties of wave propagation in the medium at the operating frequency  $f = \omega/2\pi$ . Interestingly, the topology of these contours is either open or closed as a function of whether the mass density tensor components have the same or opposite sign, respectively, with fundamentally different consequences on wave propagation<sup>48</sup>. As a landmark example of open contour topology, phononic hyperbolic metamaterials support extremely anisotropic properties, such as broadband, diffraction-free directional ray-like propagation, negative refraction, and enhanced wave-matter interaction. These phenomena arise across the entire frequency range for which the tensor elements have opposite signs, i.e., between two detuned spatially directional resonances, implying inherently broadband nature of this response. These features have been demonstrated experimentally for sound using membranes in a 2D

waveguide (Fig. 2e, bottom panel). Other acoustic implementations have been demonstrated in the context of hyperlenses<sup>49,50</sup>, as well as in elastodynamics using patterned plates<sup>51–54</sup> and asymmetric pillars<sup>55</sup>. Following recent advances in nano-optics<sup>56</sup>, sonic hyperbolic metasurfaces have been proposed<sup>57</sup>, relying on nonlocality embedded within the resonant couplings or the lattice structure, resulting in a spatial dependence of the effective compressibility. This nonlocality circumvents the constraints stemming from the inherent symmetry of the acoustic constitutive relations (Eq. 2), which prevents the existence of anisotropic compressibility tensors in the local limit.

### **Nonlocality engineering**

As mentioned in Sec. 2.1, Willis coupling coefficients are connected to a weak form of nonlocality breaking spatial symmetry, due to the fact that the dynamic effective response of the medium depends on both the local response of the unit cell and by its interaction with neighboring heterogeneities, described by the gradients of the phononic fields. Consequently, engineering nonlocal effects, along with spatial symmetry of the system, provides additional opportunities to design materials for phononic wave manipulation. A classic example of nonlocality engineering in phononics are wavelength-scaled phononic crystals<sup>1</sup>. They harness the periodicity of the lattice to tailor the dispersion of the medium in order to steer or prevent wave propagation in chosen directions within prescribed frequency ranges. This approach can be also employed to realize structure-induced negative refraction<sup>58</sup>. Nonlocality also enables bypassing the inherent limitations in efficiency and bandwidth linked to the resonant nature of passive local metasurfaces, while maintaining their reduced footprint. Indeed, unitary anomalous reflection of sound waves<sup>59</sup> and efficient vortex generation<sup>60</sup> have been achieved through the careful design of inter-cell couplings controlling nonlocal interactions, as well as broadband impedance control<sup>61–64</sup> and absorption<sup>65–67</sup> for sound and elastic waves. Engineering long range interactions in phononic metamaterials offers additional opportunities for advanced dispersion engineering<sup>68–70</sup>. For example, a roton-like dispersion has been implemented in phononic metamaterials by selectively promoting third order inter-cell couplings<sup>71–76</sup>, as shown in Fig. 2f. This feature enables multiple travelling waves with different wavenumbers at the same frequency in a homogeneous material. Remarkably, this behavior also emerges from inherently delocalized eigenmodes at zero frequency, whose existence can be precisely engineered via directed-graph theory<sup>77</sup>, resulting in anomalous dispersion cones that originate from arbitrary points in  $k$ -space.

### **Angular momentum engineering**

Beyond the design of the linear momentum dispersion  $k(\omega)$  of phononic waves through broken spatial symmetries, spatial-symmetry engineering of angular momentum is also possible. This quantity, intrinsic to acoustic and elastic waves, can be separated into two different categories: orbital  $L_{AM}$  and spin  $S_{AM}$  angular momentum. The orbital angular momentum density reads  $L_{AM} = \mathbf{r} \times \boldsymbol{\mu}$ , where  $\boldsymbol{\mu}$  is the linear momentum density. Inherently scalar, it is rooted in spatial phase gradients and is typically manifested as helicoidal wave fronts, as shown in Fig. 2g (top panels) in the case of an acoustic Bessel beam<sup>78</sup>.  $L_{AM}$  occurs both in acoustics and elastodynamics, and has been achieved using multi-source arrangements<sup>79</sup>, metasurfaces<sup>80–85</sup>, topological lattices<sup>86,87</sup>, and using spiral-shaped tube sections<sup>88,89</sup>. On the other hand, spin angular momentum  $S_{AM}$  originates from the vector nature of the field, thereby making it intrinsic to elastic waves with transverse field components<sup>90,91</sup>, and preventing its existence for homogeneous longitudinal acoustic waves. It is nevertheless possible to define a non-zero spin density  $S_{AM} \propto \Im(\mathbf{v}^* \times \mathbf{v})$  for longitudinal sound which accounts for the local elliptical polarization of the particle velocity in real space (Fig. 2g, top right panel). Upon integration over the entire medium, this quantity vanishes in homogeneous media, but it can be nonzero in the presence of field inhomogeneities<sup>78,92</sup> and for surface waves<sup>93</sup>, enabling the study of polarization-like phenomena in both acoustic<sup>94</sup> and elastic waves, such as non-trivial spin textures of phononic skyrmions<sup>95–97</sup>. By breaking the spatial symmetry of a waveguide boundaries, it is also possible to implement spin-locked sound routing<sup>98</sup>. The interaction between spin and orbital angular momentum, known as spin-orbit coupling, provides additional properties to the wave propagation, which is analogous to the chirality of optical fields. The elastodynamic version of this coupling has been implemented using twisted micro-structured mechanical materials<sup>99,100</sup> and proposed in quasi-crystals<sup>101</sup>. This twist-based design can also be extended to acoustic waves by using metastructures with dipolar resonant modes which effectively provide transverse components to the acoustic field, resulting in chirality-induced negative refraction<sup>102</sup> as shown in Fig. 2g (bottom panel). This ability to efficiently manipulate both orbital and spin angular momenta of phononic waves via spatial-symmetry engineering brings opportunities in the context of imaging<sup>103</sup>, multiplexing<sup>104</sup> and particle manipulation<sup>105–108</sup>.

## **3 Time symmetry and reciprocity**

So far, we have reviewed opportunities to engineer phononic responses through broken spatial symmetries of the microscale constituents of a medium or a metamaterial, yielding extreme control over the degree of nonlocality of the material response to phonon waves. At the macroscopic level, these asymmetries generally translate into exotic scattering properties that may be used to control how waves are reflected and transmitted through these materials. While spatial asymmetries can tailor the reflection and absorption of waves from opposite sides of a material, it is not sufficient to produce an asymmetry in the

transmission of waves between two points in space. Wave transmission between two ports generally obeys reciprocity, i.e., it is symmetric in magnitude and phase for opposite excitations at all frequencies. Consider a plane wave propagating within a linear homogeneous 1D medium over a distance  $L$ . As it propagates, it undergoes a phase shift proportional to the distance traveled and an amplitude change due to the presence of losses. These modifications do not depend on whether the wave travels to the right or to the left. Remarkably, this observation remains valid in 3D and even if the medium is inhomogeneous and arbitrarily shaped. This property, called reciprocity<sup>110</sup>, follows from Onsager principle of microscopic reversibility applied either to the scattering coefficients of a device, or to the constitutive parameters of the underlying medium, which are generalized susceptibilities in linear time-invariant media<sup>111</sup> (BOX2). Reciprocity fundamentally restricts our ability to engineer transmission asymmetry. Engineering phononic media that break this reciprocity constraint is a vibrant research area in phononics because it enables new ways to transmit elastic energy preferentially in a given direction rather than in reverse, opening opportunities to make the flow of phonons asymmetric, up to the extreme case of unidirectional transport and harvesting of phonons or heat. While reciprocity is a symmetry that extends beyond the medium itself, taking into account its interplay with sources and receivers, engineering devices that support non-reciprocal wave transmission requires breaking the underlying symmetries of the system. Recent reviews on non-reciprocity in elastodynamics and acoustics are available elsewhere<sup>110,112</sup>, so this section focuses on the role of symmetries in non-reciprocity engineering.

### 3.1 Broken spatial symmetry and nonlinearity

As just mentioned, spatial asymmetries, however complex, cannot break reciprocity for any linear time-invariant (LTI) medium that obeys microscopic reversibility<sup>110,113</sup>. The most straightforward way to break reciprocity is through the use of nonlinearities<sup>114,115</sup>. Consider a material in which the refractive index at a given location depends on the amplitude of the wave oscillation at that location, for example it has a given value for low field intensities, and switches to a higher value above a certain threshold. If we embed such a material inside a spatially asymmetric structure, we can break reciprocity by making sure that the amplitude of the field induced for excitations from the left and from the right is above and below the switching threshold, respectively, or vice versa. This effectively makes the wave interact with a different medium when excited from opposite directions, making the transmission direction-dependent, i.e., nonreciprocal. This simple mechanism has been implemented and studied fundamentally<sup>114,116–119</sup>, together with other nonlinear schemes based on other related phenomena, such as frequency conversion<sup>120–122</sup>, self-demodulation<sup>118,123</sup> or hysteresis<sup>124</sup>. The combination of spatial asymmetry and nonlinearity is a common ingredient in all these schemes, as showcased by the non-reciprocal phononic wave transmission stemming from the intrinsic nonlinear acoustic radiation pressure happening at an interface between water and air<sup>118</sup> (Fig. 3a).

### 3.2 Broken temporal symmetry

In order to observe nonreciprocal wave responses while keeping the system linear, the remaining options are either to break microscopic reversibility, or to break time-translation invariance. In the first option, we need to make the wave properties of the medium dependent on a directional bias  $\mathbf{B}_0$  that is odd upon time-reversal. This means that the propagation of the wave should directly be dependent on an external parameter, such as a constant magnetic field or electric current, whose sign reverses under the time-reversal operation. Microscopic reversibility implies that symmetry of the transmission coefficients is preserved only by reversing the bias when flipping the propagation direction. On the contrary, holding the bias constant when interchanging source and receiver positions leads to a nonreciprocal response<sup>125</sup>. While the most common way of breaking reciprocity with an external bias is to use magnetic approaches in electromagnetism<sup>126</sup>, any time-odd quantity, such as the electrical current, a linear velocity or the angular momentum can do the trick. Breaking time-translation invariance is also a viable way to effectively bias the system: by breaking the symmetry of the system under translations in time through temporal modulations it is also possible to induce strong nonreciprocal responses.

#### **Broken time-reversal symmetry**

Early works on linear nonreciprocal acoustics have considered breaking time-reversal symmetry using fluid flow or rotation<sup>127</sup>, thereby biasing the system with either linear or angular momentum beyond intrinsic magnetoacoustic effects<sup>128</sup>. In this context, the use of resonant components allows to obtain strong nonreciprocal effects with flow speeds much lower than the speed of sound. For example, Fleury *et al.* created a highly non-reciprocal acoustic circulator for audible sound using a ring cavity with a fluid spinning at a fraction of the speed of sound<sup>129</sup> (Fig. 3b), a design that was later used as a basis for theoretical and experimental investigations in topological acoustics<sup>130,131</sup>, for non-reciprocal wave manipulation in the context of janus metasurfaces<sup>132</sup> and to create non-reciprocal mode conversion in an elastic waveguide<sup>133</sup>. More recently, a different design based on nonlinear synchronization to spinning aeroacoustic limit cycles was proposed<sup>134</sup>, with the advantage of being an active mechanism, through which one can also compensate for absorption losses.

Time-reversal symmetry can also be broken in Willis media, leading to a fundamentally different kind of phononic bianisotropy. In Section 2.1, we have discussed how, in the local limit, microscopic spatial asymmetries result in Willis coupling that is *even* under time-reversal symmetry, as indicated by the requirement that the normalized effective polarizability tensor

satisfies<sup>11</sup>  $\tilde{\alpha}_{vp} = -\tilde{\alpha}_{pv}^T$ , when energy is conserved. This constraint directly translates into reciprocal scattering from a Willis particle: even in the presence of large geometrical asymmetry of the scatterer, the total extinguished power by the object must be the same for opposite excitations. Remarkably, a different form of Willis coupling can emerge within a spatially symmetric scatterer if time-reversal symmetry is broken by a constant bias<sup>135</sup>. In this case, the Willis coupling is odd-symmetric under time-reversal symmetry, meaning that the normalized off-diagonal components of the polarizability tensor are equal  $\tilde{\alpha}_{vp} = \tilde{\alpha}_{pv}^T$ . This can result in different power extinguished by the scatterer when the excitation is reversed. Odd Willis coupling has been experimentally realized using a spatially symmetric acoustic resonator with a rotating flow<sup>135</sup>, as shown in Fig. 3c. The link between spatio-temporal modulation, nonreciprocal wave transmission and odd Willis coupling was discussed in the context of elastic media by Nassar *et al.*<sup>136</sup>. Additional work on this topic proposed the implementation of nonreciprocal Willis media using moving fluids in zero-index metamaterials<sup>137</sup>. Other approaches have considered the use of active mechanisms, such as electronic feedback loops<sup>138</sup>, to induce strong nonreciprocal Willis effects, thereby improving the bandwidth, and moving beyond the theoretical limitations on Willis coefficients dictated by passivity<sup>139,140</sup>. Nonreciprocal Willis coupling has also been investigated in the presence of temperature gradients<sup>141</sup>.

Active fluids provide additional opportunities to implement nonreciprocal phonon transport, as proposed in the context of topologically protected boundary modes<sup>142–144</sup>. These effects are connected to the broader concept of odd viscosity<sup>145,146</sup>, which arises within systems for which time-reversal and mirror symmetries are broken at the microscopic scale. In practice, this behavior can stem either from single particle dynamics under an external field<sup>147,148</sup>, or from interactions between particles when the collisions break parity<sup>149</sup>, as with spinning particles<sup>150,151</sup>. Macroscopically, this property adds an antisymmetric part to the viscosity tensor of the system ( $\eta_{ijkl} \neq \eta_{klij}$ ) which, contrary to conventional viscosity, is Hermitian, i.e., not dissipative. Odd viscosity can be applied to a wide range of phenomena<sup>146</sup>, including crystalline phononic modes, where it is referred to “phonon Hall viscosity”<sup>152,153</sup>. In the context of chiral hydrodynamics, it can be associated with nonreciprocal transverse flows in compressible fluids<sup>149,151,154</sup>, which have practical consequences on wave propagation, as in the case of the shock wave depicted in Fig. 3d.

### Broken time-translation invariance

Time-reversal symmetry can be broken without violating time-translation invariance, as in the presence of a constant external bias  $\mathbf{B}_0$  that is odd-symmetric upon time-reversal. By contrast, time-translation invariance can be broken without breaking time-reversal symmetry, for example by modulating uniformly the effective index of a medium with a function that is even with respect to time (at least for one particular choice of time origin). In any case, breaking time-translation invariance requires changing the physical properties of a system in time, so that wave excitations effectively see a different system or medium at different times. While this time dependence can be arbitrary, theoretical and practical investigations have largely focused on periodic temporal modulations, which lead to Floquet systems<sup>155,156</sup>. They have the advantage of being (i) easy to model, since one can make use of band theory; (ii) quickly simulated via harmonic balance methods based on Fourier decomposition; and (iii), experimentally tractable since periodic modulations are easily generated from available electric signal generators, transducers or light sources. In Floquet systems, the dynamics are described by a periodically driven Hamiltonian  $H(t)$  obeying  $H(t) = H(t + nT_m)$ , where  $T_m$  is the modulation period and  $n$  is an integer. One of the main theoretical tools helpful to analyze these systems is the Floquet theorem<sup>155</sup>, which imposes that the allowed response of a system excited by a single tone and modulated at frequency  $\omega_m = 2\pi/T_m$  no longer exhibits just the single excitation frequency as output, but also a superposition of harmonic components spaced by  $\omega_m$ <sup>157</sup>. This is what happens within the acoustic system presented in Fig. 3e, consisting of a tight-binding lattice made of trimers of cavities whose acoustic capacitance is modulated in time, with a spatially rotating phase profile<sup>158</sup>. The corresponding Floquet harmonics appear as a repetition of the band structure along the frequency dimension. One can nevertheless simplify the picture by looking at the dynamics of a Floquet system in a stroboscopic way, namely by sampling discrete times with period  $T_m = 2\pi/\omega_m$ , because the stroboscopic evolution averages out the sub-period microscale displacements, effectively following time-independent dynamics<sup>159</sup>. The stroboscopic dynamics are described by a time-independent effective Hamiltonian  $H_{eff}$ , called the Floquet Hamiltonian. What is interesting about Floquet systems is that  $H_{eff}$  can be very different from the unmodulated Hamiltonian  $H_0$  of the system. For example, it has been shown that in the high-frequency limit  $H_{eff} = H_0 + \frac{1}{\omega_m} \sum_{n=1}^{\infty} \frac{1}{n} [H_m, H_{-m}] + O(\frac{1}{\omega_m^2})$ , where  $H_m$  is the  $m^{\text{th}}$  Fourier component of  $H(t)$ <sup>160</sup>. This means that  $H_{eff}$  differs from  $H_0$  when at least one of the commutators  $[H_m, H_{-m}]$  is non-zero, which implies that  $H(t)$  is not an even function of time, i.e., breaks time-reversal. Thus, the wave propagation in the time-modulated medium is different than in the unmodulated case, only if the drive breaks time-reversal symmetry. This is typically what happens in the modulated lattice of Fig. 3e, where the band degeneracies of the static medium are lifted upon dynamic modulation due to broken time-reversal symmetry induced by the spatially rotating phase profile<sup>158</sup>. This principle also explains why phonons can be controlled with polarized coherent light waves<sup>161</sup>, which break time-reversal symmetry either due to their linear or angular momentum, and induce non-reciprocal phonon effects. This appealing possibility is at the basis of a large body of research works aimed at engineering light-driven metastable crystalline phases and quantum effects. A notable example

is the phonon-mediated control of the magnetic properties of a lattice of spins, in order to induce giant paramagnetism<sup>162</sup>, phonon-driven magneto-valleytronics<sup>163</sup>, or ferroelectricity<sup>164</sup>. Slower Floquet modulations that break time-reversal symmetry are also relevant, as they can effectively impart some form of momentum and allow for strong nonreciprocal<sup>165–172</sup> or topological responses<sup>158,173,174</sup>, giving new opportunities for nonreciprocal acoustic devices such as robust leaky-wave antennas (Fig. 3e). In the absence of spatial gradients of the phononic properties, these Floquet modulations result in wavenumber gaps, which, albeit reciprocal, have been investigated in the context of spatial filtering<sup>175</sup>.

Beyond periodic modulation, recent works have been interested in the temporal analogues of spatial interfaces, which induce novel scattering wave phenomena, emerging when sudden, non-adiabatic changes occur to the properties of a medium without breaking spatial invariance. For example, a temporal interface can be induced in a uniform medium in which the spatially uniform refractive index is suddenly switched from one value to another. Temporal reflections and transmission emerge at such temporal interfaces, with associated temporal Fresnel coefficients and a conservation of overall momentum instead of frequency and energy, due to broken time invariance but preserved spatial symmetry<sup>176,177</sup>. Various works have investigated these phenomena, both theoretically and experimentally in 1D and 2D<sup>178–181</sup>, a landmark example being the instantaneous time-mirror<sup>178</sup>, which results in the re-focusing of water waves at the surface of a basin. Soft elastomers<sup>182,183</sup>, whose material properties depend on the medium deformation<sup>184</sup>, are also a promising platform to implement experimentally spatio-temporal interfaces for phononic waves<sup>185</sup>, in which a spatial interface travels at a finite velocity. The result of such a spatio-temporal interface are shown in Fig. 3f, demonstrating conversion of both wavenumber and frequency for a wavepacket impinging across the interface.

## 4 Time symmetry and energy conservation

So far, we have discussed how spatial and temporal symmetries can be leveraged to control phonon transport, but we have tacitly focused on quasi-conservative systems where energy losses (or gain) do not play a key role in the wave properties. In this Section, we examine how symmetry considerations become important when considering systems whose wave properties are intrinsically dependent on the careful engineering of energy balance, thereby leading to a tailored increase or decrease in the field amplitudes over time. We highlight two categories of such systems : (i) gain/loss systems, in which significant amounts of absorption losses and/or gain are purposely introduced as a parameter to control waves, and (ii) open scattering systems, in which the coupling to external ports can be leveraged to exploit an interplay between open radiation channels and the intrinsic dynamics of the closed system. In the following, we discuss the opportunities in these two contexts through examples, starting with the modal properties of systems obeying parity-time symmetry, and then discussing the scattering properties of open systems, to finish with recent approaches leveraging complex frequency excitations. We conclude this Section highlighting the interplay between symmetries and energy conservation in the elastodynamic tensors, reviewing the concepts of odd elasticity and exceptional points in conservative solids.

### 4.1 Compensating losses with symmetric gain

Early works on the use of gain and loss as an additional tuning parameter in wave physics started with the following question: can we add gain or loss to counteract undesired effects, such as the unavoidable absorption of waves close to material resonances, or the opacity of a medium due to disorder? Consider for example a closed system formed by a cavity supporting a mode that resonates at frequency  $\omega_0$ . The mode profile and the resonance frequency are respectively the eigenvector and eigenfrequency of an Hermitian eigenvalue problem described by a linear operator Hamiltonian  $H_0$ . This Hermitian formulation is always an approximation of reality, since losses are always expected in wave platforms. In practice, such a resonance always has a finite lifetime, corresponding to its exponential decay rate, i.e., an added imaginary part  $\gamma$  to  $\omega_0$ . Formally, this means that the presence of losses makes the underlying eigenvalue problem non-Hermitian. Non-Hermitian matrices have in general complex eigenvalues, although some of them can accidentally exhibit real ones. This opens an opportunity for finding systems which, despite being non-conservative, do not suffer from energy decay. The simplest instance of such systems is the one in which losses are balanced by the presence of gain, in a way that respects parity-time ( $\mathcal{P}\mathcal{T}$ ) symmetry<sup>186</sup>. Parity  $\mathcal{P}$  refers to the space inversion operation, and it is combined here with time reversal  $\mathcal{T}$ . Time-reversal changes gain to loss, and we can think of space inversion as an operation that mirrors space about the origin of the coordinate system. A system with  $\mathcal{P}\mathcal{T}$  symmetry therefore corresponds to a distribution of gain and loss that is balanced in a geometrically symmetric way. For example, our lossy resonator with eigenfrequency  $\omega_0 + i\gamma$  may be coupled to an identical resonator with gain. We may aim at compensating the decay in the first resonator by choosing the amplification rate of the second one to be exactly equal to the loss rate of the first, i.e., with intrinsic eigenfrequency  $\omega_0 - i\gamma$ . If we denote with  $\kappa$  the rate of energy coupling between them, the Hamiltonian becomes

$$H_0 = \begin{pmatrix} \omega_0 + i\gamma & \kappa \\ \kappa & \omega_0 - i\gamma \end{pmatrix}. \quad (6)$$



The corresponding eigenvalues of  $H_0$  are  $\omega_0 \pm \sqrt{\kappa^2 - \gamma^2}$  and the eigenvectors are proportional to  $[i\gamma \pm \sqrt{\kappa^2 - \gamma^2}, \kappa]^T$ . In the weak coupling limit where  $\kappa$  is small, the system supports two distinct modes, with complex conjugate eigenvalues, close to the ones of the individual resonators. One mode is mostly localized in the gain resonator, and it grows in time, while the other decays in time at the same rate, as it mostly resides in the lossy resonator. An interesting phenomenon happens in the opposite regime of strong coupling, where  $\kappa > \gamma$ . When the energy has time to circulate back and forth between the resonators before decay or gain happens, gain and loss effectively compensate each other, and the eigenvalues of the system (although described by a non-Hermitian matrix), are purely real, i.e., the modes do not grow or decay in time. This demonstrates the possibility of engineering non-Hermiticity and symmetries in a useful way, and the opportunities provided by  $\mathcal{P}\mathcal{T}$ -symmetry in the design of resonant phononic systems<sup>187–189</sup>. Working with non-Hermitian systems has other advantages: the eigenvectors of non-Hermitian matrices no longer necessarily form a complete basis, and are no longer orthogonal. Extreme cases occur where two eigenvectors become colinear, and share the same eigenvalue. Such a condition is known as an exceptional point<sup>190–195</sup>, and the associated eigenvector acts as a single attractor to which any initial condition of the system converges to. This is indeed what happens when  $\kappa = \gamma$  in Eq. (6), for which  $H_0$  is not diagonalizable any longer. The coalescence of the modes associated with the exceptional point has been evidenced in a two-level system consisting of two tightly-coupled acoustic cavities with controllable asymmetric dissipation<sup>191</sup> (Fig. 4a). Moreover, the form and topology of the Riemann sheets formed by the eigensurfaces around an exceptional point has sparked various studies, such as the effect of dynamic encircling of EPs<sup>193,196</sup> to control the mode transmission, leading to optimized sound absorption<sup>197</sup>, or the use of exceptional points for sensing<sup>198,199</sup>.

## 4.2 Exotic scattering phenomena by engineering loss and gain

Similar phenomena may be observed when looking at the signature of  $\mathcal{P}\mathcal{T}$ -symmetry on the scattering properties of a system. If a system is flux-preserving (in the sense of power flow), its scattering matrix  $S$  is unitary, i.e., its complex eigenvalues belong to the unit circle, and the outgoing power is always equal to the incident power. Losses typically affect this property, and make the scattering matrix sub-unitary. However,  $\mathcal{P}\mathcal{T}$ -symmetric systems can restore the flux conservation when operated under proper conditions (just like  $\mathcal{P}\mathcal{T}$ -symmetric cavities show no decay in the strong coupling limit). What is interesting in the case of scattering is that PT-symmetric systems can support anisotropic transmission resonances<sup>200</sup>, namely conditions under which the system is totally transparent from one side, like a lossless system, yet it can strongly reflect from the opposite side. This response has been experimentally realized in a two-port acoustic system with active components<sup>201</sup>, as shown in Fig. 4b. Under this condition, gain does not simply compensate losses ( $S_{12} = S_{21} = 1$ ), but it also cancels the reflection of the system from the lossy port ( $S_{11} = 0$ ), which is interesting from a practical standpoint. Yet, the excitation of the system from the opposite side yields strong reflections, despite supporting full transmission because of reciprocity. Here unitarity does not need to be conserved, due to the non-Hermiticity of the system and the presence of gain. By extending this concept, Rivet et al. managed to turn a complex disordered acoustic system, initially opaque, into a completely transparent one, by adding a distribution of gain and loss that was tailored to counteract the arbitrary impedance fluctuations initially present<sup>202</sup>. This directly results in a constant-pressure sound wave within the inhomogeneous sample consisting of a one-dimensional array of active acoustic scatterers (Fig. 4c). Some other potential applications related to cloaking<sup>203</sup> and directional sound emitters<sup>204</sup> have also been explored.

More insights into these phenomena can be gained by examining the connection between the  $n \times n$  closed-system Hamiltonian  $H_0$  and the  $m \times m$  scattering matrix  $S$  that we can measure after by coupling the system to  $m$  ports. This connection is given by the Mahaux-Weidenmüller formula<sup>205</sup>:  $S(\omega) = C + K[i(\omega I - (H_0 + i\Gamma_L + i\Gamma_R))]^{-1}K^T$ . Here,  $C$  is a  $m \times m$  unitary matrix representing the direct scattering path,  $K$  is the  $m \times n$  coupling matrix,  $I$  is the identity matrix and  $\Gamma_L$  and  $\Gamma_R$  are  $n \times n$  Hermitian matrices describing decay due to absorption and losses. We assume that the expression under brackets is invertible, which is equivalent to say that we operate at a real frequency  $\omega$ , which does not correspond to a bound state<sup>206,207</sup>. Due to energy conservation, one can prove that  $2\Gamma_R = K^TK$ , which reveals how coupling to the ports induce a non-Hermitian correction to  $H_0$ , which becomes  $H_0 + iK^TK/2$  if no intrinsic losses  $\Gamma_L$  are present. This correspondence between the scattering matrix and the effective non-Hermitian Hamiltonian is sketched in Fig. 4d (left panel). We note the important role of the excitation frequency  $\omega$  in the formula, which could be extended to the complex plane, revealing the importance of complex poles and zeros of  $K[i\omega I - i(H_0 + i\Gamma_L + i\Gamma_R)]^{-1}K^T$  in the scattering process. Therefore, we reach three important conclusions: (i) engineering the coupling of a closed system to a radiation continuum is another way to induce non-Hermitian properties, as in recent works<sup>208</sup>; (ii), the symmetries of  $H_0$  and of the couplings directly influence the ones of  $S$ ; and (iii), one can engineer poles and zeros of  $S$ , and even operate near them by exciting the system with complex frequencies, i.e. with exponentially growing or decaying input signals.

Typically, the addition of material gain or loss to an otherwise passive system tends to move zeros and/or poles of the scattering matrix towards the real frequency axis<sup>209</sup> (Fig. 4d, right panel). This makes the excitation of the associated scattering features possible with a standard monochromatic signal. Alternatively, one can use signals with a complex frequency, namely exponentially growing or decaying in time, which match the relevant scattering properties in the complex plane. By extending

the excitation beyond the real frequency axis, it is possible to make passive systems effectively behave as if they have controllable gain or loss, without the inherent issues of stability and energy consumption associated to active protocols which can make their practical realization challenging. First introduced in photonics<sup>210–212</sup>, these concepts of *virtual* gain and loss are rooted in the precise tailoring of the temporal shape of the impinging wave. For instance, virtual coherent absorption of elastodynamic waves has been achieved using counterpropagating signals exponentially growing in time, with a growth rate matching the leakage of the resonant inclusion<sup>213,214</sup>. Besides, a temporally decaying signal has been used to implement the transient version of the non-Hermitian skin effect<sup>215</sup>. If applied to lossy superlenses, this virtual gain permits to effectively compensate the dissipation in the system, which enables the recovery of their full subwavelength imaging potential, uniquely limited by nonlocal constraints<sup>216</sup>, as shown on Fig. 4e.

### 4.3 Odd elasticity

The stress-strain relation in linear elastic materials is uniquely defined by the elasticity tensor  $C$ . Conventionally, this relation is conservative, in the sense that the work done by the stress is independent of the deformation path, a behavior that results in a symmetric elasticity tensor:  $C_{ijkl} = C_{klij}$ . This symmetry of the elastic tensor describes Maxwell-Betti reciprocity<sup>110,146</sup>, which expresses the symmetric relation between sources and receivers in an elastic solid. In stark contrast, the presence of non-conservative microscopic interactions, such as transverse forces<sup>217</sup> or non-pairwise interactions<sup>218</sup>, leads to a non-zero anti-symmetric part of the elasticity tensor  $C_{ijkl} \neq C_{klij}$ , which is referred to as odd elasticity<sup>146,217</sup>. Obtaining these odd properties requires active elements, as in the example of Fig. 4f consisting of a beam decorated with piezoelectric patches with designed feedback loops<sup>219</sup>. In such a metamaterial, quasistatic cycles between the bending and shear modes are associated with a non-zero amount of work, which could have implications for energy harvesting and sensing. Besides, odd elasticity enables both active wave propagation and instabilities within an overdamped medium, where the domains of presence and absence of wave motion are separated by exceptional points<sup>217</sup>. It can also lead to chiral topological states<sup>220,221</sup> as well as non-Hermitian skin effects<sup>220,222</sup>, a phenomenon that describes the edge localization of almost all of the modes of a non-Hermitian system<sup>223</sup>. Non-Hermitian skin effects have also been investigated in the presence of odd mass densities<sup>224</sup>, and asymmetric couplings<sup>225–230</sup>. Such interactions effectively violate Newton's third law, meaning that they are nonreciprocal in the sense of section 3, different from the cases based on odd elasticity that do not rely on varying linear momentum. Nevertheless, some designs have been also based on active protocols, such as the feedback loops between microphones and speakers used to obtain an acoustic version of the non-Hermitian skin effect<sup>228</sup>, shown in Fig. 4g.

### 4.4 Engineering spatial Hermitian asymmetry with conservative solids

The tensorial richness of elastodynamic phenomena can be leveraged to design exceptional points in the complex wavevector space, rather than in the complex frequency space. The idea is to systematically couple the two elastic polarizations (shear and dilatation waves) in a way that forms nonorthogonal eigenmodes, and thus correspond to a non-Hermitian operator. This approach was first applied to infinitely periodic stratified media made of two isotropic, passive and lossless solids<sup>231,232</sup>. Owing to periodicity, the spatial part of the motion has a Bloch form. The non-Hermitian operator that delivers these eigenmodes is the transfer matrix, and its eigenvalues are the generally complex Bloch wavenumbers  $\{q_B\}$ . These are propagating modes if  $q_B$  is real, which implies that at the interfaces between the two solids there is a stable interconversion of energy between shear and dilatation modes. When  $q_B$  is complex, the mode undergoes spatial decay or divergence, depending on the sign of the imaginary part. A judicious design of the periodic cell can cause two Bloch modes to coalesce inside the Brillouin zone at an exceptional point which, distinct from mainstream research, is non-resonant. This approach offers a route to access non-Hermitian features without the need for material gain and loss. Physically, this occurs in open scattering problems with conservative solids and time-harmonic sources (hence correspond to real-valued frequencies) which excite Bloch modes in semi-infinite media (hence the Bloch wavenumbers may be complex to accommodate continuity conditions at the boundary). When properly tuned, these systems can give rise to anomalous wave phenomena such as negative refraction<sup>231</sup> and beam steering<sup>231,232</sup>.

The toolbox for elastic wave engineering with conservative solids can be further expanded by introducing an anisotropic constituent in the stratified media<sup>233</sup>. By rationally designing the composition, it is possible to break axial spectral symmetry, such that rightward- and leftward propagating waves are no longer symmetric. Note that this does not violate reciprocity, which requires symmetry with respect to the wavevector, not with respect to its axial component. The breakdown of this symmetry enables the coalescence of three Bloch modes. This third-order exceptional point gives to anomalous axially frozen modes, in which the transmittance in scattering problems is finite and may reach unity, in spite of the fact that the axial group velocity vanishes.

## 5 Global symmetry

The symmetries discussed in the previous section relate the microscopic structure of the medium to the properties of phonon propagation at a local level. In this section, we consider the implications of global symmetries on the behavior of waves. To meet this goal, we first take the example of topology, and show how its application to phononics connects the unit cell symmetries within the bulk of a medium to the wave behavior at its boundaries. Then, we present recent results related to the concept of duality in phononics and how they provide additional opportunities for metamaterial design beyond strict symmetry-engineering. Finally, we review the emerging concepts of twistrionics for phonons, which harness the rotation operations to engineer the macroscopic symmetries of multilayer systems, hereby enabling reconfigurable wave manipulation.

### 5.1 Phononic interface state engineering: from topology to symmetry

The boundary of a material is, to some extent, the most essential part in defining wave-matter interactions: it is the one by which we can interact with the bulk. In order to engineer devices, we can either try to perform impedance matching in order to minimize the role of interfaces as much as possible, or embrace them as an engineering knob. In this section, we describe characteristic properties of interfaces and sketch how they can be traced to topology and symmetry. Topology is an area of mathematics that connects systems invariant under continuous deformations. It permits to classify media and their associated physical properties based on simple global quantities, typically captured by integer numbers, in a way that goes beyond common symmetry-based classifications. In the context of phononics, topological approaches have been used to describe several phenomena, such as polarization textures, lattice defects, as well as phononic topological insulators. In this section, we choose to focus on selected examples linked to acoustic topological band theory, spelling out how they can be fully embedded within the paradigm of symmetry-driven phononics. For more details, we encourage the reader to refer to the extensive recent literature on the topic<sup>144,234–243</sup>.

#### 5.1.1 Interface states from a scattering perspective

It is possible to approach the origin of wave propagation at the boundaries of phononic media from a scattering perspective. When two good mirrors are placed face to face, they form a resonant cavity, where standing waves can be maintained until they are damped by losses of some kind, and whose resonant interaction with the environment is described by a scattering matrix  $S(\omega)$  (Fig. 5a, left panel). These resonant modes are obtained by requiring that a round-trip in the cavity leaves a wave in phase with itself. In other words, the dephasing  $\Delta\phi$  picked during the round-trip should be a multiple of  $2\pi$ . For a cavity of size  $L_c$ ,  $\Delta\phi = 2k(\omega)L_c + \phi_L + \phi_R$  where  $k(\omega)$  is the dispersion relation of the medium in the cavity, and  $\phi_{L/R}$  the reflection phases on the left/right sides. Now, let us consider a cavity where the walls are replaced with a phononic crystal. For frequencies  $\omega$  in a band gap, the phononic crystal acts as a frequency-dependent mirror with reflection phases  $\phi_{L/R}(\omega)$  arising from the multiple interferences on the Bragg planes of the crystal. The solutions  $\omega^*$  of  $\Delta\phi(\omega) = 0[2\pi]$  in the limit where  $L_c = 0$  correspond to edge states (also known as Tamm states, see<sup>244–246</sup>). These edge states arise at the interface between the left and right phononic crystals, thereby acting as a virtual cavity (Fig. 5a, right panel). (One of the media could be vacuum or a boundary condition.) It turns out that in some selected instances, the existence of interface states can be traced to the existence of nontrivial topological invariants in the bulk<sup>247</sup>. This link can be made precise using an approach known as the Levinson theorem, which relates the scattering phase with the number of bound states of a wave equation<sup>245,248–253</sup>. However, let us emphasise that this "bulk-boundary correspondence" is not always valid<sup>154,254–256</sup>.

#### 5.1.2 Symmetry-engineering of topological edge states

The computation of topological invariants is based on the relationship between the eigenfields of the unit cell of a periodic medium in both real and reciprocal space, which makes symmetry-based approaches an invaluable tool for topological phononics. In a nutshell, edge states often occur when the symmetry of states on both sides of an interface do not match. More precisely, let us consider a system depending on a parameter  $p$  so that a band crossing occurs where two irreducible symmetric representations cross each other at some critical value  $p_c$ . At an interface between a system with  $p < p_c$  and a system with  $p > p_c$ , a band crossing is susceptible to occur to interpolate between the band structures on both sides. This highlights the role of band degeneracies, which, upon the adequate breaking of the associated symmetries, serve as a starting point for the creation of bandgaps corresponding to topological boundary modes. For instance, Dirac cones in a honeycomb lattice present a point degeneracy related to the conservation of the time-reversal  $\mathcal{T}$  and inversion  $\mathcal{P}$  symmetries. Breaking the former yields a Chern topological insulator with non-reciprocal phononic propagation at the edge which is inherently protected against spatial defects<sup>130,131</sup> (Fig. 5b).

On the other hand, breaking the spatial inversion symmetry while preserving time-reversal symmetry, opens a bandgap in the system associated to a different kind of topological media called valley-Hall insulators<sup>257</sup>. In this case, interfaces between two mirrored inverted lattices carry edge modes whose protection is based on the conservation of an additional degree-of-freedom defined on the spatial symmetries of the lattice. Such additional degree-of-freedom, called pseudo-spin,

can be further engineered by harnessing the symmetries  $\chi$  available in the system. In particular, it allows to define a pseudo-time-reversal symmetry  $\mathcal{T}_{PS} = \chi \mathcal{T}$  such as  $\mathcal{T}_{PS}^2 = -1$ , thereby embedding phononic waves, natural bosons, with effective fermionic properties. Upon the design of the relevant pseudo-spin-orbit coupling, one can induce a symmetrical band inversion that corresponds to a topological transition within the medium. This leads to helicoidal boundary states which are robust against defects that comply with the pseudo-spin symmetry  $\chi$ . This idea has been extensively investigated in phononics across multiple platforms such as lattices of pillars with different radii<sup>258</sup>, which allows for pseudo-spins based on  $C_{6v}$  symmetry and dipolar and quadrupolar modes, whose conservation allows for wave sorting (Fig. 5c). This example illustrates a general principle that has been formalised in group-theoretical terms<sup>259,260</sup>, allowing to obtain a complete catalog of topological phononic media<sup>261</sup>.

## 5.2 Duality for phonons

The general definition of a symmetry, namely a transformation that leaves the system invariant, leaves room for other kinds of symmetries, which can be less straightforward, or somewhat hidden. An example is given in Fig. 5d, where two different mass-spring chains share an identical band structure at the scale of the Brillouin zone, albeit the absence of any conventional symmetrical relation between them. These “hidden symmetries” may look at first glance to be accidental. To understand their nature, it is convenient to consider an entire family of systems continuously depending on parameter  $p$  rather than looking at each system individually. Formally, to define a symmetry, the structure of the system of interest needs to be encoded into a mathematical object such as a Hamiltonian or a dynamical matrix  $H$ , or  $H(p)$  for an explicit dependence on the parameter  $p$ . Besides, transformations are generally encoded into operators  $U$ , that are symmetries of  $H$  provided that  $UHU^{-1} = H$ . In this case, it is implicit that parameters are the same in  $H = H(p)$  on both sides of the equation. In this framework, dualities can be seen as symmetries that also change parameter  $p$  associated to the system. For instance, let us introduce a function  $u(p)$  and say that  $U$  is a duality when  $UH(p)U^{-1} = H(u(p))$ . Interestingly, at specific fixed points  $p^*$  of  $u$  such that  $u(p^*) = p^*$ , known as self-dual points, the duality reduces into a conventional symmetry operation. For example, consider the mechanical structure known as a twisted Kagome lattice<sup>262</sup> shown in Fig. 5e. In this case, the parameter  $p = \theta$  is the twist angle, and  $H$  stands for the dynamical matrix of the phonons. The duality operator  $U$  shuffles the vibrational degrees-of-freedom in the unit cell as shown in Fig. 5e (inset), and  $u(p) = -p$ . Because of the duality within the family of twisted lattices, the band structures of dual systems are identical. Other examples of mechanical systems dualities can be found in<sup>263–265</sup>, including a systematic way to construct them<sup>263</sup>. In addition, the abstract Maxwell duality between floppy modes and states of self-stress<sup>266–269</sup>, can also translate into a physical duality between parallelogram tilings and fiber networks<sup>266</sup>, see Fig. 5f. Beyond the iso-spectrality of dual media, duality operations put additional constraints on the self-dual configuration, similarly to conventional symmetries. More generally, wave dualities have consequences on the macroscopic elastic properties<sup>270</sup>, affect the propagation of waves at interfaces<sup>271</sup> as well as topological edge and corner states<sup>272–274</sup>. They also lead to pseudo-spin degeneracies unusual in mechanics that can be exploited to perform information processing using non-Abelian geometric phases<sup>262</sup>.

## 5.3 Twistronics for phonons

In the Section 2.3, we have discussed how engineering the anisotropy of a medium’s elementary inclusions can tailor its macroscopic phononic properties. In the case of multi-layer systems, it is possible to further combine the spatial symmetries associated of each layer, thereby providing more opportunities to manipulate phononic waves. In this context, inter-layer rotations are a powerful tool to selectively and reconfigurably break the symmetries of the global multi-layer system. In turn, this can result in new physical effects, as in electronics where the concepts related to twistronics<sup>275</sup> are actively investigated. Recent advances have shown transposing these ideas to phononics is a valuable strategy to better and tunable wave control. For instance, in the case of multilayer phononic crystals, the interplay between each layers’ spatial symmetries, mediated by the twist operation, also leads to a tunable control of the dispersion. Specifically, emerging moiré patterns with long-range periodicity at specific twist angles are responsible for flat bands in the dispersion relation of the twisted multilayer, which are tightly linked to field localization and strong resonant behavior<sup>276–280</sup>. Although the periodicity of moiré patterns only exists for a discrete set of twist angles, it does not limit the potential of rotations for symmetry engineering. Indeed, twist-driven topological effects<sup>281,282</sup> and tunable gauge fields for negative refraction<sup>283</sup> have been demonstrated over large angular ranges, as showcased on Fig. 5g. Rotations are also relevant in the context of twisted hyperbolic metasurfaces. First proposed in photonics<sup>284</sup>, the latter consists of strongly coupled monolayers with hyperbolic dispersion which are rotated with respect to each other<sup>285,286</sup>. By controlling the twist angle, the bilayer system undergoes a topological transition between open and closed frequency contours for a broad range of frequencies, enabling a broadband tunability of the directionality and localization of the wave propagation. In particular, the transition *magic-angle* corresponds to a canalization regime with enhanced wave matter interaction. This topological transition can also be driven by actual moiré patterns emerging from the symmetry mismatch between the underlying lattice and a rotated anisotropic spatial modulation of the unit cells properties, as demonstrated on an elastodynamic platform<sup>55</sup>. Moreover, twisted shear hyperbolic metasurfaces provides additional opportunities to control both the Hermitian and non-Hermitian features of the wave propagations<sup>287</sup>. Indeed, breaking the orthogonality between two detuned resonances, results in shear hyperbolic waves, originally observed with phonon-polaritons at the surface of natural

monoclinic crystals<sup>288</sup>. For a fixed twist angle, the principal axis of the hyperbolic medium rotates with frequency, and the spatial distribution of loss does not match the contour's symmetry. At the operating frequency, this translates into an effective material tensor  $\boldsymbol{\tau}$ , whose Hermitian part is diagonal while its non-Hermitian part presents some off-diagonal terms (Fig. 5h). Using the twist between two detuned hyperbolic metasurfaces, this effect can be maximized, and directly results in a screwed hyperbolic field profile where some branches are overdamped and others enhanced in comparison to a conventional hyperbolic medium.

## Outlook

As showcased throughout this review, a symmetry-driven approach turns out to be a successful paradigm for advanced manipulation of phononic fields, across a wide range of domains and scales. Starting from straightforward spatial symmetry engineering at the scale of the meta-atoms, it is possible to create acoustic and elastodynamic media with unconventional properties, stemming from bi- or tri-anisotropy, both local and nonlocal by design. These artificial materials enable the design of devices for enhanced sensing, wave guiding and steering relevant to the domains of noise control, audio-engineering, architecture acoustics, underwater imaging and communication, and biomedical acoustics. Extreme anisotropy, which can be found in hyperbolic metasurfaces and engineered acoustic chirality have also enabled extreme control of acoustic fields, providing opportunities for better sensing, focusing and particle manipulation. Combining both spatial and time symmetries lead to the emergence of nonreciprocal phononic meta-structures, which enables acoustic analogues of isolators, circulators and phonon diodes. In most cases, these devices require active elements for the temporal modulation of their effective properties or to induce momentum bias via flow within the system. With these active schemes come issues of stability and speed which require additional research for many practical applications. In that regard, the future development of multi-physics concepts like electro- or magneto-momentum couplings has a great potential to push the levels of reconfigurability of phononic media beyond what is currently possible. In particular, the ability to implement extremely fast modulations of the global properties of the medium over a large scale would allow the investigation of out-of-equilibrium physical phenomena and the use time as an extra tuning parameter in the context of 4D metamaterials<sup>289</sup>. Reconfigurable acoustic metasurfaces paired with optimization protocols have also proven to be crucial tool for wavefield shaping, hereby allowing advanced multiplexing of acoustic communication in complex environments<sup>290</sup>. Alternatively, the use of active matter<sup>144</sup>, as well as flexible soft elastomers<sup>182–184</sup> to modify the properties of the propagating medium opens the door to complex dynamic wave phenomena for which analogies with the behavior of biological tissues and soft robotics could be drawn. Moreover, as exemplified by the thriving domain of topological phononics, symmetry-engineered meta-structures serve as a powerful tabletop platform for the study of fundamental phenomena. In that context, new ideas and implementations linked to non-Abelian, non-Hermitian and non-linear topological phenomena, as well as topological defects and disordered topological phases have emerged as a means to control acoustic and optical fields<sup>291,292</sup>. These are promising directions for the exploration of active and reconfigurable topological media, which, along with the concepts of wave dualities, are relevant for next-generation computation and telecommunications applications built on topologically robust devices. We finally note that the symmetry-driven approach described in the context of mechanical continua also applies to actual phonons, namely the vibrations of atomic lattices. In the near-infrared optical frequencies, they interact with photons to create quasi-particles called phonon-polaritons, whose symmetry-related properties, such as hyperbolicity for instance, are currently under extensive theoretical and experimental study<sup>293</sup>. Controlling the propagation of these hybrid surface waves, either via twisted multi-layer systems or artificial patterning, is at the heart of modern nano-photonics and future investigations combining both spatial and time symmetries, such as Floquet polaritonics, are promising research directions. In addition to phonon-polaritons, the intrinsic chirality of phonons in natural alpha-quartz has been recently measured via inelastic X-ray scattering<sup>294</sup>. That work provides experimental proof of a new degree-of-freedom for phononic excitations of relevance to topological physics and multi-physics phenomena combining light, sound and electronic properties. While this review has primarily focused on meta-structures to control dynamic wave propagation, it is important to note that the symmetry-engineering approach is also relevant to static mechanical metamaterials where the careful design of unit cells allows to manipulate the 0-frequency response of the medium<sup>295,296</sup>, leading to better control and mitigation of fracture, elastic buckling and impact response of these systems. Adding active components to such artificial media opens new avenues in the broader context of autonomous metamaterial-based machines which are of relevance for sensing, shape-morphing and object manipulation, as well as for the physical modelling of biological systems. Finally, going beyond symmetry-based approaches, the use of inverse design and machine learning protocols to implement artificial meta-structures are efficient complementary tools for advanced phononic wave manipulation<sup>297</sup>.

### Acknowledgements

A.A. and S.Y. were supported by the National Science Foundation Science and Technology Center 'New Frontiers of Sound', the Department of Defense and the Simons Foundation. G.S. acknowledges funding by the European Union (ERC, EXCEPTIONAL, Project No. 101045494). M.R.H. acknowledges support from Office of Naval Research under Award No. N00014-23-1-2660. R.F. acknowledges funding by the Swiss National Science Foundation under the Eccellenza Award 181232. M.F. and V.V.

acknowledge partial support from the France Chicago center through a FACCTS grant. V.V. acknowledges partial support from the Army Research Office under grant W911NF-22-2-0109 and W911NF-23-1-0212, the National Science Foundation through the Center for Living Systems (grant no. 2317138), the National Institute for Theory and Mathematics in Biology, the Chan Zuckerberg Foundation and the Simons Foundation.

#### Author contributions

All authors contributed substantially to the discussion of the content. A.A. and M.R.H. initiated the project. S.Y., R.F., G.S., M.F., V.V. researched the data and wrote the respective sections of the article. All authors reviewed and edited the manuscript.

#### Competing interests

The authors declare no competing interests.

## References

1. Deymier, P. A. *Acoustic metamaterials and phononic crystals*, vol. 173 (Springer Science & Business Media, 2013).
2. Haberman, M. R. & Guild, M. D. Acoustic metamaterials. *Phys. Today* **69**, 42–48 (2016).
3. Ma, G. & Sheng, P. Acoustic metamaterials: From local resonances to broad horizons. *Sci. Adv.* **2**, e1501595 (2016).
4. Cummer, S. A., Christensen, J. & Alù, A. Controlling sound with acoustic metamaterials. *Nat. Rev. Mater.* **1**, 1–13 (2016).
5. Assouar, B. *et al.* Acoustic metasurfaces. *Nat. Rev. Mater.* **3**, 460–472, DOI: [10.1038/s41578-018-0061-4](https://doi.org/10.1038/s41578-018-0061-4) (2018).
6. Craster, R. V., Guenneau, S. R., Muamer, K. & Wegener, M. Mechanical metamaterials. *Reports on Prog. Phys.* (2023).
7. Pierce, A. D. *Acoustics, 3<sup>rd</sup> Edition* (Springer, Cham, Switzerland, 2019).
8. Achenbach, J. D. *Wave propagation in elastic solids* (Elsevier, Amsterdam, Netherlands, 1973).
9. Willis, J. R. Variational and related methods for the overall properties of composites. *Adv. Appl. Mech.* **21**, 1–78 (1981).
10. Willis, J. R. The construction of effective relations for waves in a composite. *Comptes Rendus Mécanique* **340**, 181 – 192, DOI: <https://doi.org/10.1016/j.crme.2012.02.001> (2012). Recent Advances in Micromechanics of Materials.
11. Quan, L., Ra’di, Y., Sounas, D. L. & Alù, A. Maximum Willis Coupling in Acoustic Scatterers. *Phys. Rev. Lett.* **120**, 254301, DOI: [10.1103/PhysRevLett.120.254301](https://doi.org/10.1103/PhysRevLett.120.254301) (2018).
12. Willis, J. R. Effective constitutive relations for waves in composites and metamaterials. *Proc. R. Soc. Lond. A Math. Phys. Eng. Sci.* **467**, 1865–1879, DOI: [10.1098/rspa.2010.0620](https://doi.org/10.1098/rspa.2010.0620) (2011).
13. Milton, G. W., Briane, M. & Willis, J. R. On cloaking for elasticity and physical equations with a transformation invariant form. *New J. Phys.* **8**, 248 (2006).
14. Milton, G. W. & Willis, J. R. On modifications of Newton’s second law and linear continuum elastodynamics. *Proc. R. Soc. Lond. A Math. Phys. Eng. Sci.* **463**, 855–880, DOI: [10.1098/rspa.2006.1795](https://doi.org/10.1098/rspa.2006.1795) (2007).
15. Sieck, C. F., Alù, A. & Haberman, M. R. Origins of Willis coupling and acoustic bianisotropy in acoustic metamaterials through source-driven homogenization. *Phys. Rev. B* **96**, 104303, DOI: [10.1103/PhysRevB.96.104303](https://doi.org/10.1103/PhysRevB.96.104303) (2017).
16. Pernas-Salomón, R., Haberman, M. R., Norris, A. N. & Shmuel, G. The electromomentum effect in piezoelectric Willis scatterers. *Wave Motion* 102797, DOI: <https://doi.org/10.1016/j.wavemoti.2021.102797> (2021).
17. Liu, Y. *et al.* Willis metamaterial on a structured beam. *Phys. Rev. X* **9**, 011040 (2019).
18. Muhlestein, M. B., Sieck, C. F., Alù, A. & Haberman, M. R. Reciprocity, passivity and causality in Willis materials. *Proc. R. Soc. Lond. A Math. Phys. Eng. Sci.* **472**, DOI: [10.1098/rspa.2016.0604](https://doi.org/10.1098/rspa.2016.0604) (2016).
19. Pernas-Salomón, R. & Shmuel, G. Fundamental Principles for Generalized Willis Metamaterials. *Phys. Rev. Appl.* **14**, 064005, DOI: [10.1103/PhysRevApplied.14.064005](https://doi.org/10.1103/PhysRevApplied.14.064005) (2020).
20. Koo, S., Cho, C., Jeong, J.-h. & Park, N. Acoustic omni meta-atom for decoupled access to all octants of a wave parameter space. *Nat. Commun.* **7**, 13012 (2016).
21. Fietz, C. & Shvets, G. Current-driven metamaterial homogenization. *Phys. B: Condens. Matter* **405**, 2930 – 2934, DOI: <https://doi.org/10.1016/j.physb.2010.01.006> (2010). Proceedings of the Eighth International Conference on Electrical Transport and Optical Properties of Inhomogeneous Media.
22. Willis, J. R. Exact effective relations for dynamics of a laminated body. *Mech. Mater.* **41**, 385–393, DOI: [http://dx.doi.org/10.1016/j.mechmat.2009.01.010](https://doi.org/10.1016/j.mechmat.2009.01.010) (2009).

23. Melnikov, A. *et al.* Acoustic meta-atom with experimentally verified maximum Willis coupling. *Nat. Commun.* **10**, 3148, DOI: [10.1038/s41467-019-10915-5](https://doi.org/10.1038/s41467-019-10915-5) (2019).
24. Merkel, A., Romero-García, V., Groby, J.-P., Li, J. & Christensen, J. Unidirectional zero sonic reflection in passive pt-symmetric willis media. *Phys. Rev. B* **98**, 201102 (2018).
25. Peng, Y.-G., Mazor, Y. & Alù, A. Fundamentals of acoustic willis media. *Wave Motion* **112**, 102930 (2022).
26. Esfahlani, H., Mazor, Y. & Alù, A. Homogenization and design of acoustic Willis metasurfaces. *Phys. Rev. B* **103**, 054306 (2021).
27. Muhlestein, M. B., Sieck, C. F., Wilson, P. S. & Haberman, M. R. Experimental evidence of Willis coupling in a one-dimensional effective material element. *Nat. Commun.* **8**, 15625 EP – (2017).
28. Lau, J., Tang, S. T., Yang, M. & Yang, Z. Coupled Decorated Membrane Resonators with Large Willis Coupling. *Phys. Rev. Appl.* **12**, 014032, DOI: [10.1103/PhysRevApplied.12.014032](https://doi.org/10.1103/PhysRevApplied.12.014032) (2019).
29. Sounas, D. L. & Alù, A. Extinction symmetry for reciprocal objects and its implications on cloaking and scattering manipulation. *Opt. Lett.* **39**, 4053–4056 (2014).
30. Lawrence, A. J., Goldsberry, B. M., Wallen, S. P. & Haberman, M. R. Numerical study of acoustic focusing using a bianisotropic acoustic lens. *The J. Acoust. Soc. Am.* **148**, EL365–EL369, DOI: [10.1121/10.0002137](https://doi.org/10.1121/10.0002137) (2020).
31. Li, J. *et al.* Highly efficient generation of angular momentum with cylindrical bianisotropic metasurfaces. *Phys. Rev. Appl.* **11**, 024016 (2019).
32. Li, J., Shen, C., D'iaz-Rubio, A., Tretyakov, S. A. & Cummer, S. A. Systematic design and experimental demonstration of bianisotropic metasurfaces for scattering-free manipulation of acoustic wavefronts. *Nat. Commun.* **9**, 1342, DOI: [10.1038/s41467-018-03778-9](https://doi.org/10.1038/s41467-018-03778-9) (2018).
33. Hao, Y., Shen, Y., Groby, J.-P. & Li, J. Experimental demonstration of Willis coupling for elastic torsional waves. *Wave Motion* **112**, 102931 (2022).
34. Chen, Y. & Haberman, M. R. Controlling displacement fields in polar Willis solids via gauge transformations. *Phys. Rev. Lett.* **130**, 147201 (2023).
35. Sepehrihahnama, S., Oberst, S., Chiang, Y. K. & Powell, D. A. Willis coupling-induced acoustic radiation force and torque reversal. *Phys. Rev. Lett.* **129**, 174501 (2022).
36. Mason, W. P. *Piezoelectric crystals and their application to ultrasonics.* (Van Nostrand, New York, 1950).
37. Pernas-Salomón, R. & Shmuel, G. Symmetry breaking creates electro-momentum coupling in piezoelectric metamaterials. *J. Mech. Phys. Solids* **134**, 103770, DOI: <https://doi.org/10.1016/j.jmps.2019.103770> (2020).
38. Kosta, M., Muhafra, A., Pernas-Salómon, R., Shmuel, G. & Amir, O. Maximizing the electromomentum coupling in piezoelectric laminates. *Int. J. Solids Struct.* **254-255**, 111909, DOI: <https://doi.org/10.1016/j.ijsolstr.2022.111909> (2022).
39. Muhafra, A., Kosta, M., Torrent, D., Pernas-Salomón, R. & Shmuel, G. Homogenization of piezoelectric planar Willis materials undergoing antiplane shear. *Wave Motion* **108**, 102833, DOI: <https://doi.org/10.1016/j.wavemoti.2021.102833> (2022).
40. Muhafra, K., Haberman, M. R. & Shmuel, G. Discrete one-dimensional models for the electromomentum coupling. *Phys. Rev. Appl.* **20**, 014042, DOI: [10.1103/PhysRevApplied.20.014042](https://doi.org/10.1103/PhysRevApplied.20.014042) (2023).
41. Danawe, H. & Tol, S. Electro-momentum coupling tailored in piezoelectric metamaterials with resonant shunts. *APL Mater.* **11**, 091118, DOI: [10.1063/5.0165267](https://doi.org/10.1063/5.0165267). [https://pubs.aip.org/aip/apm/article-pdf/doi/10.1063/5.0165267/18141427/091118\\_1\\_5.0165267.pdf](https://pubs.aip.org/aip/apm/article-pdf/doi/10.1063/5.0165267/18141427/091118_1_5.0165267.pdf).
42. Huynh, H. D. *et al.* Maximizing electro-momentum coupling in generalized 2d Willis metamaterials. *Extrem. Mech. Lett.* **61**, 101981, DOI: <https://doi.org/10.1016/j.eml.2023.101981> (2023).
43. Lee, J.-H., Zhang, Z. & Gu, G. X. Maximum electro-momentum coupling in piezoelectric metamaterial scatterers. *J. Appl. Phys.* **132**, 125108 (2022).
44. Lee, J.-H., Zhang, Z. & Gu, G. X. Reaching new levels of wave scattering via piezoelectric metamaterials and electro-momentum coupling. *The J. Acoust. Soc. Am.* **153**, A163–A163, DOI: [10.1121/10.0018518](https://doi.org/10.1121/10.0018518) (2023).
45. Wallen, S. P., Casali, M. A., Goldsberry, B. M. & Haberman, M. R. Polarizability of electromomentum coupled scatterers. In *Proceedings of Meetings on Acoustics*, vol. 46, DOI: [10.1121/2.0001597](https://doi.org/10.1121/2.0001597) (AIP Publishing, 2022).

46. Christensen, J. & de Abajo, F. J. G. Anisotropic metamaterials for full control of acoustic waves. *Phys. Rev. Lett.* **108**, 124301, DOI: [10.1103/PhysRevLett.108.124301](https://doi.org/10.1103/PhysRevLett.108.124301) (2012).
47. Milton, G. W. & Willis, J. R. On modifications of Newton's second law and linear continuum elastodynamics. *Proc. Royal Soc. A: Math. Phys. Eng. Sci.* **463**, 855–880 (2007).
48. Krishnamoorthy, H. N., Jacob, Z., Narimanov, E., Kretzschmar, I. & Menon, V. M. Topological transitions in metamaterials. *Science* **336**, 205–209 (2012).
49. Li, J., Fok, L., Yin, X., Bartal, G. & Zhang, X. Experimental demonstration of an acoustic magnifying hyperlens. *Nat. Mater.* **8**, 931–934 (2009).
50. Lu, D. & Liu, Z. Hyperlenses and metalenses for far-field super-resolution imaging. *Nat. Commun.* **3**, 1205 (2012).
51. Oh, J. H., Min Seung, H. & Young Kim, Y. A truly hyperbolic elastic metamaterial lens. *Appl. Phys. Lett.* **104** (2014).
52. Zhu, R., Chen, Y., Wang, Y., Hu, G. & Huang, G. A single-phase elastic hyperbolic metamaterial with anisotropic mass density. *The J. Acoust. Soc. Am.* **139**, 3303–3310 (2016).
53. Lee, H., Oh, J. H., Seung, H. M., Cho, S. H. & Kim, Y. Y. Extreme stiffness hyperbolic elastic metamaterial for total transmission subwavelength imaging. *Sci. Rep.* **6**, 24026 (2016).
54. Dong, H.-W., Zhao, S.-D., Wang, Y.-S. & Zhang, C. Broadband single-phase hyperbolic elastic metamaterials for super-resolution imaging. *Sci. Rep.* **8**, 2247 (2018).
55. Yves, S. *et al.* Moiré-driven topological transitions and extreme anisotropy in elastic metasurfaces. *Adv. Sci.* **9**, 2200181 (2022).
56. Gomez-Diaz, J. & Alu, A. Flatland optics with hyperbolic metasurfaces. *ACS Photonics* **3**, 2211–2224 (2016).
57. Quan, L. & Alù, A. Hyperbolic sound propagation over nonlocal acoustic metasurfaces. *Phys. Rev. Lett.* **123**, 244303 (2019).
58. Kaina, N., Lemoult, F., Fink, M. & Lerosey, G. Negative refractive index and acoustic superlens from multiple scattering in single negative metamaterials. *Nature* **525**, 77–81 (2015).
59. Quan, L. & Alù, A. Passive acoustic metasurface with unitary reflection based on nonlocality. *Phys. Rev. Appl.* **11**, 054077 (2019).
60. Hou, Z., Ding, H., Wang, N., Fang, X. & Li, Y. Acoustic vortices via nonlocal metagratings. *Phys. Rev. Appl.* **16**, 014002 (2021).
61. Zhu, H., Patnaik, S., Walsh, T. F., Jared, B. H. & Semperlotti, F. Nonlocal elastic metasurfaces: Enabling broadband wave control via intentional nonlocality. *Proc. Natl. Acad. Sci.* **117**, 26099–26108 (2020).
62. Zhou, Z., Huang, S., Li, D., Zhu, J. & Li, Y. Broadband impedance modulation via non-local acoustic metamaterials. *Natl. Sci. Rev.* **9**, nwab171 (2022).
63. Zhou, H.-T., Fu, W.-X., Wang, Y.-F. & Wang, Y.-S. High-efficiency ultrathin nonlocal waterborne acoustic metasurface. *Phys. Rev. Appl.* **15**, 044046 (2021).
64. Yang, T., Lin, Z. & Yang, T. Experimental evidence of high-efficiency nonlocal waterborne acoustic metasurfaces. *Adv. Eng. Mater.* **25**, 2200805 (2023).
65. Zhu, Y. *et al.* Nonlocal acoustic metasurface for ultrabroadband sound absorption. *Phys. Rev. B* **103**, 064102 (2021).
66. Nair, S., Jokar, M. & Semperlotti, F. Nonlocal acoustic black hole metastructures: Achieving broadband and low frequency passive vibration attenuation. *Mech. Syst. Signal Process.* **169**, 108716 (2022).
67. Yuan, X., Li, Q., Wu, C., Huang, Y. & Wu, X. Broadband ventilated metamaterial absorber from non-local coupling. *Extrem. Mech. Lett.* **66**, 102119 (2024).
68. Kazemi, A. *et al.* Drawing dispersion curves: Band structure customization via nonlocal phononic crystals. *Phys. Rev. Lett.* **131**, 176101 (2023).
69. Moore, D., Sambles, J., Hibbins, A., Starkey, T. & Chaplain, G. Acoustic surface modes on metasurfaces with embedded next-nearest-neighbor coupling. *Phys. Rev. B* **107**, 144110 (2023).
70. Chaplain, G., Hooper, I., Hibbins, A. & Starkey, T. Reconfigurable elastic metamaterials: Engineering dispersion with beyond nearest neighbors. *Phys. Rev. Appl.* **19**, 044061 (2023).
71. Chen, Y., Kadic, M. & Wegener, M. Roton-like acoustical dispersion relations in 3d metamaterials. *Nat. Commun.* **12**, 3278 (2021).



72. Iglesias Martínez, J. A. *et al.* Experimental observation of roton-like dispersion relations in metamaterials. *Sci. Adv.* **7**, eabm2189 (2021).
73. Wang, K., Chen, Y., Kadic, M., Wang, C. & Wegener, M. Nonlocal interaction engineering of 2d roton-like dispersion relations in acoustic and mechanical metamaterials. *Commun. Mater.* **3**, 35 (2022).
74. Zhu, Z. *et al.* Observation of multiple rotons and multidirectional roton-like dispersion relations in acoustic metamaterials. *New J. Phys.* **24**, 123019 (2022).
75. Chen, Y. *et al.* Phonon transmission through a nonlocal metamaterial slab. *Commun. Phys.* **6**, 75 (2023).
76. Chen, Y. *et al.* Observation of chirality-induced roton-like dispersion in a 3d micropolar elastic metamaterial. *Adv. Funct. Mater.* 2302699 (2023).
77. Bossart, A. & Fleury, R. Extreme spatial dispersion in nonlocally resonant elastic metamaterials. *Phys. Rev. Lett.* **130**, 207201 (2023).
78. Bliokh, K. Y. & Nori, F. Spin and orbital angular momenta of acoustic beams. *Phys. Rev. B* **99**, 174310 (2019).
79. Wang, S., Ma, G. & Chan, C. T. Topological transport of sound mediated by spin-redirected geometric phase. *Sci. Adv.* **4**, eaaq1475 (2018).
80. Jiang, X., Li, Y., Liang, B., Cheng, J.-c. & Zhang, L. Convert acoustic resonances to orbital angular momentum. *Phys. Rev. Lett.* **117**, 034301 (2016).
81. Fu, Y. *et al.* Sound vortex diffraction via topological charge in phase gradient metagratings. *Sci. Adv.* **6**, eaba9876 (2020).
82. Gao, S., Li, Y., Ma, C., Cheng, Y. & Liu, X. Emitting long-distance spiral airborne sound using low-profile planar acoustic antenna. *Nat. Commun.* **12**, 2006 (2021).
83. Fan, X.-D. & Zhang, L. Acoustic orbital angular momentum hall effect and realization using a metasurface. *Phys. Rev. Res.* **3**, 013251 (2021).
84. Jiang, X., Ta, D. & Wang, W. Modulation of orbital-angular-momentum symmetry of nondiffractive acoustic vortex beams and realization using a metasurface. *Phys. Rev. Appl.* **14**, 034014 (2020).
85. Zhang, H. *et al.* Topologically crafted spatiotemporal vortices in acoustics. *Nat. Commun.* **14**, 6238 (2023).
86. Wang, Q. *et al.* Vortex states in an acoustic weyl crystal with a topological lattice defect. *Nat. Commun.* **12**, 3654 (2021).
87. Lu, J., Qiu, C., Ke, M. & Liu, Z. Valley vortex states in sonic crystals. *Phys. Rev. Lett.* **116**, 093901 (2016).
88. Chaplain, G., De Ponti, J. & Craster, R. Elastic orbital angular momentum. *Phys. Rev. Lett.* **128**, 064301 (2022).
89. Chaplain, G. J., De Ponti, J. M. & Starkey, T. A. Elastic orbital angular momentum transfer from an elastic pipe to a fluid. *Commun. Phys.* **5**, 279 (2022).
90. Long, Y., Ren, J. & Chen, H. Intrinsic spin of elastic waves. *Proc. Natl. Acad. Sci.* **115**, 9951–9955 (2018).
91. Bliokh, K. Y. Elastic spin and orbital angular momenta. *Phys. Rev. Lett.* **129**, 204303 (2022).
92. Burns, L., Bliokh, K. Y., Nori, F. & Dressel, J. Acoustic versus electromagnetic field theory: scalar, vector, spinor representations and the emergence of acoustic spin. *New J. Phys.* **22**, 053050 (2020).
93. Bliokh, K. Y. & Nori, F. Transverse spin and surface waves in acoustic metamaterials. *Phys. Rev. B* **99**, 020301 (2019).
94. Muelas-Hurtado, R. D. *et al.* Observation of polarization singularities and topological textures in sound waves. *Phys. Rev. Lett.* **129**, 204301 (2022).
95. Ge, H. *et al.* Observation of acoustic skyrmions. *Phys. Rev. Lett.* **127**, 144502 (2021).
96. Hu, P. *et al.* Observation of localized acoustic skyrmions. *Appl. Phys. Lett.* **122** (2023).
97. Cao, L., Wan, S., Zeng, Y., Zhu, Y. & Assouar, B. Observation of phononic skyrmions based on hybrid spin of elastic waves. *Sci. Adv.* **9**, eadf3652 (2023).
98. Long, Y. *et al.* Realization of acoustic spin transport in metasurface waveguides. *Nat. Commun.* **11**, 4716 (2020).
99. Frenzel, T., Kadic, M. & Wegener, M. Three-dimensional mechanical metamaterials with a twist. *Science* **358**, 1072–1074 (2017).
100. Frenzel, T., Köpfler, J., Jung, E., Kadic, M. & Wegener, M. Ultrasound experiments on acoustical activity in chiral mechanical metamaterials. *Nat. Commun.* **10**, 3384 (2019).

101. Chen, Y., Kadic, M., Guenneau, S. & Wegener, M. Isotropic chiral acoustic phonons in 3d quasicrystalline metamaterials. *Phys. Rev. Lett.* **124**, 235502 (2020).
102. Wang, S. *et al.* Spin-orbit interactions of transverse sound. *Nat. Commun.* **12**, 6125 (2021).
103. Noetinger, G. *et al.* Superresolved imaging based on spatiotemporal wave-front shaping. *Phys. Rev. Appl.* **19**, 024032 (2023).
104. Shi, C., Dubois, M., Wang, Y. & Zhang, X. High-speed acoustic communication by multiplexing orbital angular momentum. *Proc. Natl. Acad. Sci.* **114**, 7250–7253 (2017).
105. Baresch, D., Thomas, J.-L. & Marchiano, R. Observation of a single-beam gradient force acoustical trap for elastic particles: Acoustical tweezers. *Phys. Rev. Lett.* **116**, 024301, DOI: [10.1103/PhysRevLett.116.024301](https://doi.org/10.1103/PhysRevLett.116.024301) (2016).
106. Melde, K., Mark, A. G., Qiu, T. & Fischer, P. Holograms for acoustics. *Nature* **537**, 518–522 (2016).
107. Cox, L., Melde, K., Croxford, A., Fischer, P. & Drinkwater, B. W. Acoustic hologram enhanced phased arrays for ultrasonic particle manipulation. *Phys. Rev. Appl.* **12**, 064055 (2019).
108. Melde, K. *et al.* Compact holographic sound fields enable rapid one-step assembly of matter in 3d. *Sci. Adv.* **9**, eadf6182 (2023).
109. Shen, C. *et al.* Broadband acoustic hyperbolic metamaterial. *Phys. Rev. Lett.* **115**, 254301 (2015).
110. Nassar, H. *et al.* Nonreciprocity in acoustic and elastic materials. *Nat. Rev. Mater.* **5**, 667–685 (2020).
111. Onsager, L. Reciprocal relations in irreversible processes. I. *Phys. Rev.* **37**, 405 (1931).
112. Zangeneh-Nejad, F. & Fleury, R. Active times for acoustic metamaterials. *Rev. Phys.* **4**, 100031 (2019).
113. Fleury, R. *Breaking temporal symmetries in metamaterials and metasurfaces*. Ph.D. thesis (2015).
114. Liang, B., Guo, X., Tu, J., Zhang, D. & Cheng, J. An acoustic rectifier. *Nat. Mater.* **9**, 989–992 (2010).
115. Blanchard, A., Sapsis, T. P. & Vakakis, A. F. Non-reciprocity in nonlinear elastodynamics. *J. Sound Vib.* **412**, 326–335 (2018).
116. Sounas, D. L. & Alu, A. Time-reversal symmetry bounds on the electromagnetic response of asymmetric structures. *Phys. Rev. Lett.* **118**, 154302 (2017).
117. Darabi, A. *et al.* Broadband passive nonlinear acoustic diode. *Phys. Rev. B* **99**, 214305 (2019).
118. Devaux, T., Cebrecos, A., Richoux, O., Pagneux, V. & Tournat, V. Acoustic radiation pressure for nonreciprocal transmission and switch effects. *Nat. Commun.* **10**, 3292 (2019).
119. Liang, B., Yuan, B. & Cheng, J.-c. Acoustic diode: Rectification of acoustic energy flux in one-dimensional systems. *Phys. Rev. Lett.* **103**, 104301 (2009).
120. Boechler, N., Theocharis, G. & Daraio, C. Bifurcation-based acoustic switching and rectification. *Nat. Mater.* **10**, 665–668 (2011).
121. Meng, X. & Liu, S. Roton-enabled mechanical diode at extremely low frequency. *J. Appl. Mech.* **91**, 011010–1 (2024).
122. Guo, X., Lissek, H. & Fleury, R. Observation of non-reciprocal harmonic conversion in real sounds. *Commun. Phys.* **6**, 93 (2023).
123. Devaux, T., Tournat, V., Richoux, O. & Pagneux, V. Asymmetric acoustic propagation of wave packets via the self-demodulation effect. *Phys. Rev. Lett.* **115**, 234301 (2015).
124. Librandi, G., Tubaldi, E. & Bertoldi, K. Programming nonreciprocity and reversibility in multistable mechanical metamaterials. *Nat. Commun.* **12**, 3454 (2021).
125. Cummer, S. A. Selecting the direction of sound transmission. *Science* **343**, 495–496 (2014).
126. Caloz, C. *et al.* Electromagnetic nonreciprocity. *Phys. Rev. Appl.* **10**, 047001 (2018).
127. Roux, P., de Rosny, J., Tanter, M. & Fink, M. The aharonov-bohm effect revisited by an acoustic time-reversal mirror. *Phys. Rev. Lett.* **79**, 3170 (1997).
128. Kittel, C. Interaction of spin waves and ultrasonic waves in ferromagnetic crystals. *Phys. Rev.* **110**, 836 (1958).
129. Fleury, R., Sounas, D. L., Sieck, C. F., Haberman, M. R. & Alù, A. Sound isolation and giant linear nonreciprocity in a compact acoustic circulator. *Science* **343**, 516–519 (2014).

130. Khanikaev, A. B., Fleury, R., Mousavi, S. H. & Alu, A. Topologically robust sound propagation in an angular-momentum-biased graphene-like resonator lattice. *Nat. Commun.* **6**, 8260 (2015).
131. Ding, Y. *et al.* Experimental demonstration of acoustic chern insulators. *Phys. Rev. Lett.* **122**, 014302 (2019).
132. Zhu, Y. *et al.* Janus acoustic metascreen with nonreciprocal and reconfigurable phase modulations. *Nat. Commun.* **12**, 7089 (2021).
133. Goldsberry, B. M., Wallen, S. P. & Haberman, M. R. Nonreciprocity and mode conversion in a spatiotemporally modulated elastic wave circulator. *Phys. Rev. Appl.* **17**, 034050 (2022).
134. Pederghana, T., Faure-Beaulieu, A., Fleury, R. & Noiray, N. Loss-compensated non-reciprocal scattering based on synchronization. *Nat. Commun.* **15**, 7436 (2024).
135. Quan, L., Yves, S., Peng, Y., Esfahlani, H. & Alù, A. Odd Willis coupling induced by broken time-reversal symmetry. *Nat. Commun.* **12**, 2615 (2021).
136. Nassar, H., Xu, X., Norris, A. & Huang, G. Modulated phononic crystals: Non-reciprocal wave propagation and willis materials. *J. Mech. Phys. Solids* **101**, 10–29 (2017).
137. Quan, L., Sounas, D. L. & Alù, A. Nonreciprocal Willis coupling in zero-index moving media. *Phys. Rev. Lett.* **123**, 064301 (2019).
138. Chen, Y., Li, X., Hu, G., Haberman, M. R. & Huang, G. An active mechanical willis meta-layer with asymmetric polarizabilities. *Nat. Commun.* **11**, 3681 (2020).
139. Cho, C., Wen, X., Park, N. & Li, J. Acoustic Willis meta-atom beyond the bounds of passivity and reciprocity. *Commun. Phys.* **4**, 82 (2021).
140. Wen, X., Yip, H. K., Cho, C., Li, J. & Park, N. Acoustic amplifying diode using nonreciprocal Willis coupling. *Phys. Rev. Lett.* **130**, 176101 (2023).
141. Olivier, C. *et al.* Nonreciprocal and even Willis couplings in periodic thermoacoustic amplifiers. *Phys. Rev. B* **104**, 184109 (2021).
142. Souslov, A., Van Zuiden, B. C., Bartolo, D. & Vitelli, V. Topological sound in active-liquid metamaterials. *Nat. Phys.* **13**, 1091–1094 (2017).
143. Sone, K. & Ashida, Y. Anomalous topological active matter. *Phys. Rev. Lett.* **123**, 205502 (2019).
144. Shankar, S., Souslov, A., Bowick, M. J., Marchetti, M. C. & Vitelli, V. Topological active matter. *Nat. Rev. Phys.* **4**, 380–398 (2022).
145. Avron, J. Odd viscosity. *J. Stat. Phys.* **92**, 543–557 (1998).
146. Fruchart, M., Scheibner, C. & Vitelli, V. Odd viscosity and odd elasticity. *Annu. Rev. Condens. Matter Phys.* **14**, 471–510 (2023).
147. Kaufman, A. N. Plasma viscosity in a magnetic field. *The Phys. Fluids* **3**, 610–616, DOI: [10.1063/1.1706096](https://doi.org/10.1063/1.1706096) (1960).
148. Markovich, T. & Lubensky, T. C. Odd viscosity in active matter: microscopic origin and 3d effects. *Phys. Rev. Lett.* **127**, 048001 (2021).
149. Han, M. *et al.* Fluctuating hydrodynamics of chiral active fluids. *Nat. Phys.* **17**, 1260–1269 (2021).
150. Banerjee, D., Souslov, A., Abanov, A. G. & Vitelli, V. Odd viscosity in chiral active fluids. *Nat. Commun.* **8**, 1573 (2017).
151. Soni, V. *et al.* The odd free surface flows of a colloidal chiral fluid. *Nat. Phys.* **15**, 1188–1194 (2019).
152. Heidari, S., Cortijo, A. & Asgari, R. Hall viscosity for optical phonons. *Phys. Rev. B* **100**, 165427 (2019).
153. Barkeshli, M., Chung, S. B. & Qi, X.-L. Dissipationless phonon hall viscosity. *Phys. Rev. B* **85**, 245107 (2012).
154. Souslov, A., Dasbiswas, K., Fruchart, M., Vaikuntanathan, S. & Vitelli, V. Topological waves in fluids with odd viscosity. *Phys. Rev. Lett.* **122**, 128001 (2019).
155. Floquet, G. Sur les équations différentielles linéaires à coefficients périodiques. In *Annales scientifiques de l'École normale supérieure*, vol. 12, 47–88 (1883).
156. Rudner, M. S. & Lindner, N. H. The floquet engineer's handbook. *arXiv preprint arXiv:2003.08252* (2020).
157. Sambe, H. Steady states and quasienergies of a quantum-mechanical system in an oscillating field. *Phys. Rev. A* **7**, 2203 (1973).

158. Fleury, R., Khanikaev, A. B. & Alu, A. Floquet topological insulators for sound. *Nat. Commun.* **7**, 11744 (2016).
159. Shirley, J. H. Solution of the schrödinger equation with a hamiltonian periodic in time. *Phys. Rev.* **138**, B979 (1965).
160. Bukov, M., D'Alessio, L. & Polkovnikov, A. Universal high-frequency behavior of periodically driven systems: from dynamical stabilization to floquet engineering. *Adv. Phys.* **64**, 139–226 (2015).
161. Disa, A. S., Nova, T. F. & Cavalleri, A. Engineering crystal structures with light. *Nat. Phys.* **17**, 1087–1092 (2021).
162. Juraschek, D. M., Neuman, T. & Narang, P. Giant effective magnetic fields from optically driven chiral phonons in 4 f paramagnets. *Phys. Rev. Res.* **4**, 013129 (2022).
163. Shin, D. *et al.* Phonon-driven spin-floquet magneto-valleytronics in mos2. *Nat. Commun.* **9**, 638 (2018).
164. Radaelli, P. G. Breaking symmetry with light: Ultrafast ferroelectricity and magnetism from three-phonon coupling. *Phys. Rev. B* **97**, 085145 (2018).
165. Fleury, R., Sounas, D. L. & Alù, A. Subwavelength ultrasonic circulator based on spatiotemporal modulation. *Phys. Rev. B* **91**, 174306 (2015).
166. Shen, C., Zhu, X., Li, J. & Cummer, S. A. Nonreciprocal acoustic transmission in space-time modulated coupled resonators. *Phys. Rev. B* **100**, 054302 (2019).
167. Chen, Y. *et al.* Nonreciprocal wave propagation in a continuum-based metamaterial with space-time modulated resonators. *Phys. Rev. Appl.* **11**, 064052 (2019).
168. Wang, Y. *et al.* Observation of nonreciprocal wave propagation in a dynamic phononic lattice. *Phys. Rev. Lett.* **121**, 194301 (2018).
169. Marconi, J. *et al.* Experimental observation of nonreciprocal band gaps in a space-time-modulated beam using a shunted piezoelectric array. *Phys. Rev. Appl.* **13**, 031001 (2020).
170. Chen, Z. *et al.* Efficient nonreciprocal mode transitions in spatiotemporally modulated acoustic metamaterials. *Sci. Adv.* **7**, eabj1198 (2021).
171. Shao, L. *et al.* Electrical control of surface acoustic waves. *Nat. Electron.* **5**, 348–355 (2022).
172. Wen, X. *et al.* Unidirectional amplification with acoustic non-hermitian space- time varying metamaterial. *Commun. Phys.* **5**, 18 (2022).
173. Darabi, A., Ni, X., Leamy, M. & Alù, A. Reconfigurable floquet elastodynamic topological insulator based on synthetic angular momentum bias. *Sci. Adv.* **6**, eaba8656 (2020).
174. Chen, Z.-x. *et al.* Observation of acoustic floquet  $\pi$  modes in a time-varying lattice. *Phys. Rev. B* **109**, L020302 (2024).
175. Trainiti, G. *et al.* Time-periodic stiffness modulation in elastic metamaterials for selective wave filtering: Theory and experiment. *Phys. Rev. Lett.* **122**, 124301 (2019).
176. Caloz, C. & Deck-Leger, Z.-L. Spacetime metamaterials—part ii: Theory and applications. *IEEE Transactions on Antennas Propag.* **68**, 1583–1598 (2019).
177. Moussa, H. *et al.* Observation of temporal reflection and broadband frequency translation at photonic time interfaces. *Nat. Phys.* **19**, 863–868 (2023).
178. Bacot, V., Labousse, M., Eddi, A., Fink, M. & Fort, E. Time reversal and holography with spacetime transformations. *Nat. Phys.* **12**, 972–977 (2016).
179. Bacot, V., Durey, G., Eddi, A., Fink, M. & Fort, E. Phase-conjugate mirror for water waves driven by the faraday instability. *Proc. Natl. Acad. Sci.* **116**, 8809–8814 (2019).
180. Mouet, V., Apffel, B. & Fort, E. Comprehensive refractive manipulation of water waves using electrostriction. *Proc. Natl. Acad. Sci.* **120**, e2216828120 (2023).
181. Apffel, B., Wildeman, S., Eddi, A. & Fort, E. Experimental implementation of wave propagation in disordered time-varying media. *Phys. Rev. Lett.* **128**, 094503 (2022).
182. Lanoy, M., Lemoult, F., Eddi, A. & Prada, C. Dirac cones and chiral selection of elastic waves in a soft strip. *Proc. Natl. Acad. Sci.* **117**, 30186–30190 (2020).
183. Delory, A., Lemoult, F., Lanoy, M., Eddi, A. & Prada, C. Soft elastomers: A playground for guided waves. *The J. Acoust. Soc. Am.* **151**, 3343–3358 (2022).

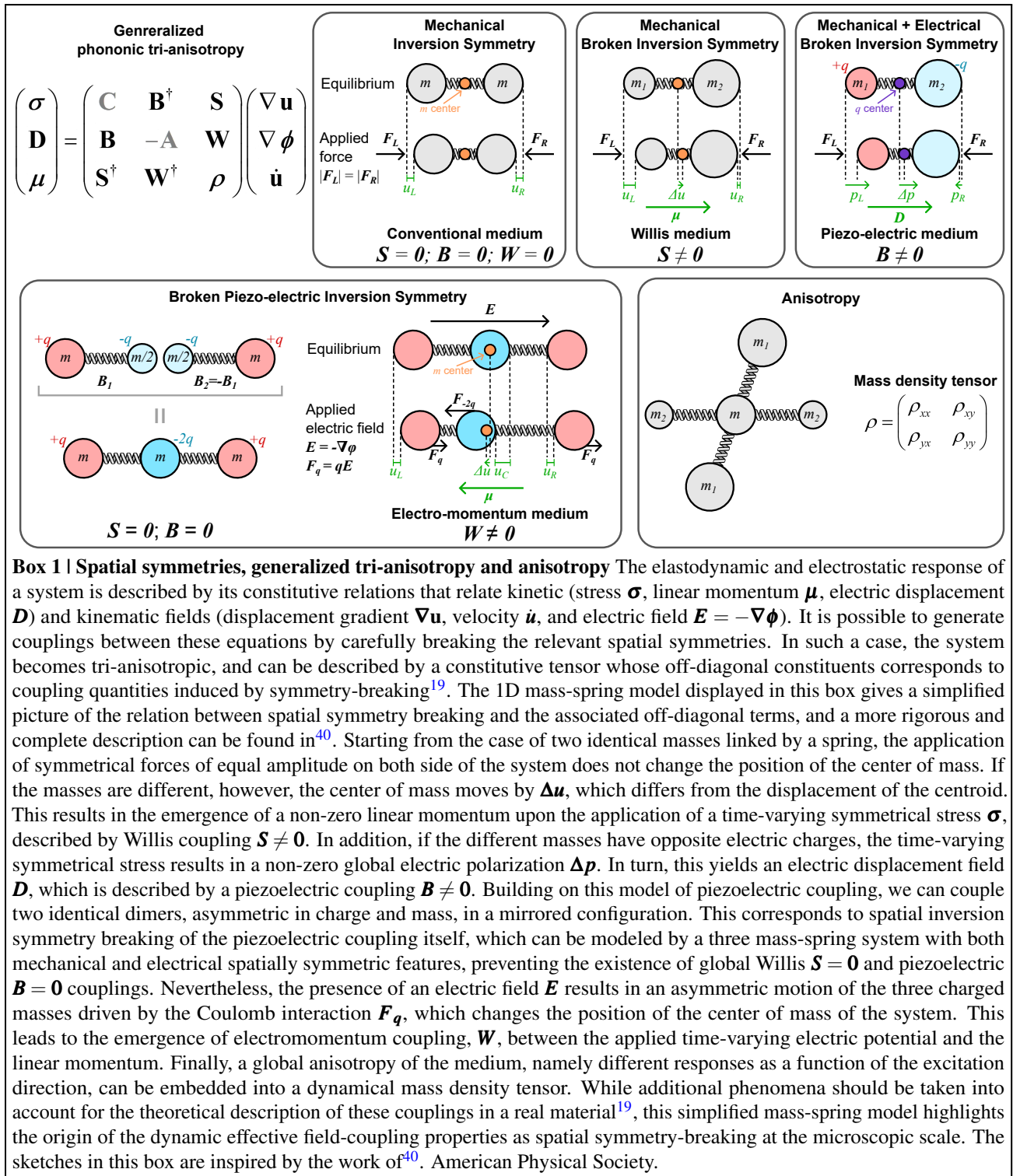
184. Delory, A., Lemoult, F., Eddi, A. & Prada, C. Guided elastic waves in a highly-stretched soft plate. *Extrem. Mech. Lett.* **61**, 102018 (2023).
185. Delory, A. *et al.* Elastic wavepackets crossing a space-time interface. *arXiv preprint arXiv:2406.15100* (2024).
186. Bender, C. M. & Boettcher, S. Real spectra in non-hermitian hamiltonians having p t symmetry. *Phys. Rev. Lett.* **80**, 5243 (1998).
187. Zhu, X., Ramezani, H., Shi, C., Zhu, J. & Zhang, X. P t-symmetric acoustics. *Phys. Rev. X* **4**, 031042 (2014).
188. Christensen, J., Willatzen, M., Velasco, V. & Lu, M.-H. Parity-time synthetic phononic media. *Phys. Rev. Lett.* **116**, 207601 (2016).
189. Fleury, R., Sounas, D. L. & Alu, A. Parity-time symmetry in acoustics: theory, devices, and potential applications. *IEEE J. Sel. Top. Quantum Electron.* **22**, 121–129 (2016).
190. Shi, C. *et al.* Accessing the exceptional points of parity-time symmetric acoustics. *Nat. Commun.* **7**, 11110 (2016).
191. Ding, K., Ma, G., Xiao, M., Zhang, Z. & Chan, C. T. Emergence, coalescence, and topological properties of multiple exceptional points and their experimental realization. *Phys. Rev. X* **6**, 021007 (2016).
192. Ding, K., Ma, G., Zhang, Z. & Chan, C. T. Experimental demonstration of an anisotropic exceptional point. *Phys. Rev. Lett.* **121**, 085702 (2018).
193. Tang, W. *et al.* Exceptional nexus with a hybrid topological invariant. *Science* **370**, 1077–1080 (2020).
194. Tang, W., Ding, K. & Ma, G. Direct measurement of topological properties of an exceptional parabola. *Phys. Rev. Lett.* **127**, 034301 (2021).
195. Tang, W., Ding, K. & Ma, G. Realization and topological properties of third-order exceptional lines embedded in exceptional surfaces. *Nat. Commun.* **14**, 6660 (2023).
196. Elbaz, G., Pick, A., Moiseyev, N. & Shmuel, G. Encircling exceptional points of bloch waves: mode conversion and anomalous scattering. *J. Phys. D: Appl. Phys.* (2022).
197. Achilleos, V., Theocharis, G., Richoux, O. & Pagneux, V. Non-hermitian acoustic metamaterials: Role of exceptional points in sound absorption. *Phys. Rev. B* **95**, 144303 (2017).
198. Shmuel, G. & Moiseyev, N. Linking scalar elastodynamics and non-hermitian quantum mechanics. *Phys. Rev. Appl.* **13**, 024074, DOI: [10.1103/PhysRevApplied.13.024074](https://doi.org/10.1103/PhysRevApplied.13.024074) (2020).
199. Wiersig, J. Review of exceptional point-based sensors. *Photonics Res.* **8**, 1457, DOI: [10.1364/prj.396115](https://doi.org/10.1364/prj.396115) (2020).
200. Ge, L., Chong, Y. & Stone, A. D. Conservation relations and anisotropic transmission resonances in one-dimensional pt-symmetric photonic heterostructures. *Phys. Rev. A* **85**, 023802 (2012).
201. Fleury, R., Sounas, D. & Alu, A. An invisible acoustic sensor based on parity-time symmetry. *Nat. Commun.* **6**, 5905 (2015).
202. Rivet, E. *et al.* Constant-pressure sound waves in non-hermitian disordered media. *Nat. Phys.* **14**, 942–947 (2018).
203. Li, H.-x. *et al.* Ultrathin acoustic parity-time symmetric metasurface cloak. *Research* (2019).
204. Magariyachi, T., Arias Casals, H., Herrero, R., Botey, M. & Staliunas, K. Pt-symmetric helmholtz resonator dipoles for sound directivity. *Phys. Rev. B* **103**, 094201 (2021).
205. Mahaux, C. & Weidenmüller, H. A. Shell-model approach to nuclear reactions. *Shell-model approach to nuclear reactions* (1969).
206. Hsu, C. W., Zhen, B., Stone, A. D., Joannopoulos, J. D. & Soljačić, M. Bound states in the continuum. *Nat. Rev. Mater.* **1**, 1–13 (2016).
207. Huang, L. *et al.* Acoustic resonances in non-hermitian open systems. *Nat. Rev. Phys.* **6**, 11–27 (2024).
208. Franca, S., Könye, V., Hassler, F., van den Brink, J. & Fulga, C. Non-hermitian physics without gain or loss: the skin effect of reflected waves. *Phys. Rev. Lett.* **129**, 086601 (2022).
209. Krasnok, A. *et al.* Anomalies in light scattering. *Adv. Opt. Photonics* **11**, 892–951 (2019).
210. Baranov, D. G., Krasnok, A. & Alu, A. Coherent virtual absorption based on complex zero excitation for ideal light capturing. *Optica* **4**, 1457–1461 (2017).
211. Kim, S., Lepeshov, S., Krasnok, A. & Alù, A. Beyond bounds on light scattering with complex frequency excitations. *Phys. Rev. Lett.* **129**, 203601 (2022).

212. Ra'di, Y., Krasnok, A. & Alù, A. Virtual critical coupling. *ACS Photonics* **7**, 1468–1475 (2020).
213. Trainiti, G., Ra'di, Y., Ruzzene, M. & Alù, A. Coherent virtual absorption of elastodynamic waves. *Sci. Adv.* **5**, eaaw3255 (2019).
214. Rasmussen, C., Rosa, M. I., Lewton, J. & Ruzzene, M. A lossless sink based on complex frequency excitations. *Adv. Sci.* **10**, 2301811 (2023).
215. Gu, Z. *et al.* Transient non-hermitian skin effect. *Nat. Commun.* **13**, 7668 (2022).
216. Kim, S., Peng, Y.-G., Yves, S. & Alù, A. Loss compensation and superresolution in metamaterials with excitations at complex frequencies. *Phys. Rev. X* **13**, 041024 (2023).
217. Scheibner, C. *et al.* Odd elasticity. *Nat. Phys.* **16**, 475–480 (2020).
218. Brandenbourger, M., Scheibner, C., Veenstra, J., Vitelli, V. & Coullais, C. Limit cycles turn active matter into robots. *arXiv preprint arXiv:2108.08837* (2021).
219. Chen, Y., Li, X., Scheibner, C., Vitelli, V. & Huang, G. Realization of active metamaterials with odd micropolar elasticity. *Nat. Commun.* **12**, 5935 (2021).
220. Scheibner, C., Irvine, W. T. & Vitelli, V. Non-hermitian band topology and skin modes in active elastic media. *Phys. Rev. Lett.* **125**, 118001 (2020).
221. Fossati, M., Scheibner, C., Fruchart, M. & Vitelli, V. Odd elasticity and topological waves in active surfaces. *Phys. Rev. E* **109**, 024608 (2024).
222. Wang, Y., Wu, Q., Tian, Y. & Huang, G. Non-hermitian wave dynamics of odd plates: Microstructure design and theoretical modelling. *J. Mech. Phys. Solids* **182**, 105462 (2024).
223. Hatano, N. & Nelson, D. R. Localization transitions in non-hermitian quantum mechanics. *Phys. Rev. Lett.* **77**, 570 (1996).
224. Wu, Q. *et al.* Active metamaterials for realizing odd mass density. *Proc. Natl. Acad. Sci.* **120**, e2209829120 (2023).
225. Ghatak, A., Brandenbourger, M., Van Wezel, J. & Coullais, C. Observation of non-hermitian topology and its bulk–edge correspondence in an active mechanical metamaterial. *Proc. Natl. Acad. Sci.* **117**, 29561–29568 (2020).
226. Gao, P., Willatzen, M. & Christensen, J. Anomalous topological edge states in non-hermitian piezophononic media. *Phys. Rev. Lett.* **125**, 206402 (2020).
227. Zhang, L. *et al.* Acoustic non-hermitian skin effect from twisted winding topology. *Nat. Commun.* **12**, 6297 (2021).
228. Zhang, X., Tian, Y., Jiang, J.-H., Lu, M.-H. & Chen, Y.-F. Observation of higher-order non-hermitian skin effect. *Nat. Commun.* **12**, 5377 (2021).
229. Wang, W., Wang, X. & Ma, G. Non-hermitian morphing of topological modes. *Nature* **608**, 50–55 (2022).
230. Wang, W., Hu, M., Wang, X., Ma, G. & Ding, K. Experimental realization of geometry-dependent skin effect in a reciprocal two-dimensional lattice. *Phys. Rev. Lett.* **131**, 207201 (2023).
231. Lustig, B., Elbaz, G., Muhafrá, A. & Shmuel, G. Anomalous energy transport in laminates with exceptional points. *J. Mech. Phys. Solids* 103719, DOI: <https://doi.org/10.1016/j.jmps.2019.103719> (2019).
232. Mokhtari, A. A., Lu, Y., Zhou, Q., Amirkhizi, A. V. & Srivastava, A. Scattering of in-plane elastic waves at metamaterial interfaces. *Int. J. Eng. Sci.* **150**, 103278, DOI: <https://doi.org/10.1016/j.ijengsci.2020.103278> (2020).
233. Fishman, A., Elbaz, G., Varma, T. V. & Shmuel, G. Third-order exceptional points and frozen modes in planar elastic laminates. *J. Mech. Phys. Solids* **186**, 105590, DOI: <https://doi.org/10.1016/j.jmps.2024.105590> (2024).
234. Ma, G., Xiao, M. & Chan, C. T. Topological phases in acoustic and mechanical systems. *Nat. Rev. Phys.* **1**, 281–294 (2019).
235. Huber, S. D. Topological mechanics. *Nat. Phys.* **12**, 621–623 (2016).
236. Miniaci, M. & Pal, R. Design of topological elastic waveguides. *J. Appl. Phys.* **130** (2021).
237. Zhang, X., Xiao, M., Cheng, Y., Lu, M.-H. & Christensen, J. Topological sound. *Commun. Phys.* **1**, 97 (2018).
238. Xue, H., Yang, Y. & Zhang, B. Topological acoustics. *Nat. Rev. Mater.* **7**, 974–990 (2022).
239. Ni, X., Yves, S., Krasnok, A. & Alu, A. Topological metamaterials. *Chem. Rev.* **123**, 7585–7654 (2023).
240. Yves, S., Ni, X. & Alù, A. Topological sound in two dimensions. *Annals New York Acad. Sci.* **1517**, 63–77 (2022).

241. Coulais, C., Fleury, R. & van Wezel, J. Topology and broken hermiticity. *Nat. Phys.* **17**, 9–13 (2021).
242. Ding, K., Fang, C. & Ma, G. Non-hermitian topology and exceptional-point geometries. *Nat. Rev. Phys.* **4**, 745–760 (2022).
243. Zhu, W. *et al.* Topological phononic metamaterials. *Reports on Prog. Phys.* (2023).
244. Kaliteevski, M. *et al.* Tamm plasmon-polaritons: Possible electromagnetic states at the interface of a metal and a dielectric bragg mirror. *Phys. Rev. B* **76**, 165415 (2007).
245. Xiao, M., Zhang, Z. & Chan, C. T. Surface impedance and bulk band geometric phases in one-dimensional systems. *Phys. Rev. X* **4**, 021017 (2014).
246. Levy, E. & Akkermans, E. Topological boundary states in 1d: An effective fabry-perot model. *The Eur. Phys. J. Special Top.* **226**, 1563–1582 (2017).
247. Hasan, M. Z. & Kane, C. L. Colloquium: topological insulators. *Rev. Mod. Phys.* **82**, 3045 (2010).
248. Fulga, I. C., Hassler, F. & Akhmerov, A. R. Scattering theory of topological insulators and superconductors. *Phys. Rev. B* **85**, 165409 (2012).
249. Fulga, I., Hassler, F., Akhmerov, A. & Beenakker, C. Scattering formula for the topological quantum number of a disordered multimode wire. *Phys. Rev. B* **83**, 155429 (2011).
250. Graf, G. M. & Porta, M. Bulk-edge correspondence for two-dimensional topological insulators. *Commun. Math. Phys.* **324**, 851–895 (2013).
251. Sellers, I. *et al.* Strong coupling of light with a and b excitons in gan microcavities grown on silicon. *Phys. Rev. B* **73**, 033304 (2006).
252. Bräunlich, G., Graf, G. & Ortelli, G. Equivalence of topological and scattering approaches to quantum pumping. *Commun. Math. Phys.* **295**, 243–259 (2010).
253. Kellendonk, J. & Richard, S. The topological meaning of levinson’s theorem, half-bound states included. *J. Phys. A: Math. Theor.* **41**, 295207 (2008).
254. Tauber, C., Delplace, P. & Venaille, A. A bulk-interface correspondence for equatorial waves. *J. Fluid Mech.* **868**, R2 (2019).
255. Tauber, C., Delplace, P. & Venaille, A. Anomalous bulk-edge correspondence in continuous media. *Phys. Rev. Res.* **2**, 013147 (2020).
256. Gangaraj, S. A. H. & Monticone, F. Physical violations of the bulk-edge correspondence in topological electromagnetics. *Phys. Rev. Lett.* **124**, 153901 (2020).
257. Lu, J. *et al.* Observation of topological valley transport of sound in sonic crystals. *Nat. Phys.* **13**, 369–374 (2017).
258. He, C. *et al.* Acoustic topological insulator and robust one-way sound transport. *Nat. Phys.* **12**, 1124–1129 (2016).
259. Bradlyn, B. *et al.* Topological quantum chemistry. *Nature* **547**, 298–305 (2017).
260. Cano, J. & Bradlyn, B. Band representations and topological quantum chemistry. *Annu. Rev. Condens. Matter Phys.* **12**, 225–246 (2021).
261. Xu, Y. *et al.* Catalog of topological phonon materials. *Science* **384**, eadf8458 (2024).
262. Fruchart, M., Zhou, Y. & Vitelli, V. Dualities and non-abelian mechanics. *Nature* **577**, 636–640 (2020).
263. Fruchart, M., Yao, C. & Vitelli, V. Systematic generation of hamiltonian families with dualities. *Phys. Rev. Res.* **5**, 023099 (2023).
264. Lei, Q.-L., Tang, F., Hu, J.-D., Ma, Y.-q. & Ni, R. Duality, hidden symmetry, and dynamic isomerism in 2d hinge structures. *Phys. Rev. Lett.* **129**, 125501 (2022).
265. Yang, Z.-J. & Wang, Y.-Z. Non-abelian mechanics of elastic waves in kagome metamaterials with internal microstructures. *Proc. Royal Soc. A* **479**, 20220713 (2023).
266. Zhou, D., Zhang, L. & Mao, X. Topological boundary floppy modes in quasicrystals. *Phys. Rev. X* **9**, 021054 (2019).
267. Kane, C. L. & Lubensky, T. C. Topological boundary modes in isostatic lattices. *Nat. Phys.* **10**, 39–45 (2014).
268. McInerney, J., Chen, B. G.-g., Theran, L., Santangelo, C. D. & Rocklin, D. Z. Hidden symmetries generate rigid folding mechanisms in periodic origami. *Proc. Natl. Acad. Sci.* **117**, 30252–30259 (2020).

269. Czajkowski, M. & Rocklin, D. Z. Duality and sheared analytic response in mechanism-based metamaterials. *Phys. Rev. Lett.* **132**, 068201 (2024).
270. Fruchart, M. & Vitelli, V. Symmetries and dualities in the theory of elasticity. *Phys. Rev. Lett.* **124**, 248001 (2020).
271. Gonella, S. Symmetry of the phononic landscape of twisted kagome lattices across the duality boundary. *Phys. Rev. B* **102**, 140301 (2020).
272. Danawe, H., Li, H., Al Ba'ba'a, H. & Tol, S. Existence of corner modes in elastic twisted kagome lattices. *Phys. Rev. B* **104**, L241107 (2021).
273. Azizi, P., Sarkar, S., Sun, K. & Gonella, S. Dynamics of self-dual kagome metamaterials and the emergence of fragile topology. *Phys. Rev. Lett.* **130**, 156101 (2023).
274. Allein, F. *et al.* Strain topological metamaterials and revealing hidden topology in higher-order coordinates. *Nat. Commun.* **14**, 6633 (2023).
275. Carr, S. *et al.* Twistronics: Manipulating the electronic properties of two-dimensional layered structures through their twist angle. *Phys. Rev. B* **95**, 075420 (2017).
276. López, M. R., Peñaranda, F., Christensen, J. & San-Jose, P. Flat bands in magic-angle vibrating plates. *Phys. Rev. Lett.* **125**, 214301 (2020).
277. Deng, Y. *et al.* Magic-angle bilayer phononic graphene. *Phys. Rev. B* **102**, 180304 (2020).
278. Gardezi, S. M., Pirie, H., Carr, S., Dorrell, W. & Hoffman, J. E. Simulating twistronics in acoustic metamaterials. *2D Mater.* **8**, 031002 (2021).
279. Martí-Sabaté, M. & Torrent, D. Dipolar localization of waves in twisted phononic crystal plates. *Phys. Rev. Appl.* **15**, L011001 (2021).
280. López, M. R., Zhang, Z., Torrent, D. & Christensen, J. Theory of holey twistsonic media. *Commun. Mater.* **3**, 99 (2022).
281. Rosa, M. I., Ruzzene, M. & Prodan, E. Topological gaps by twisting. *Commun. Phys.* **4**, 130 (2021).
282. Wu, S.-Q. *et al.* Higher-order topological states in acoustic twisted Moiré superlattices. *Phys. Rev. Appl.* **17**, 034061 (2022).
283. Yang, Y. *et al.* Demonstration of negative refraction induced by synthetic gauge fields. *Sci. Adv.* **7**, eabj2062 (2021).
284. Hu, G., Krasnok, A., Mazor, Y., Qiu, C.-W. & Alù, A. Moiré hyperbolic metasurfaces. *Nano Lett.* **20**, 3217–3224 (2020).
285. Yves, S., Peng, Y.-G. & Alù, A. Topological Lifshitz transition in twisted hyperbolic acoustic metasurfaces. *Appl. Phys. Lett.* **121** (2022).
286. Han, C. *et al.* Nonlocal acoustic Moiré hyperbolic metasurfaces. *Adv. Mater.* 2311350 (2024).
287. Yves, S., Galiffi, E., Ni, X., Renzi, E. M. & Alù, A. Twist-induced hyperbolic shear metasurfaces. *Phys. Rev. X* **14**, 021031 (2024).
288. Passler, N. C. *et al.* Hyperbolic shear polaritons in low-symmetry crystals. *Nature* **602**, 595–600 (2022).
289. Engheta, N. Four-dimensional optics using time-varying metamaterials. *Science* **379**, 1190–1191 (2023).
290. Bourdeloux, C., Fink, M. & Lemoult, F. Solution to the cocktail party problem: A time-reversal active metasurface for multipoint focusing. *Phys. Rev. Appl.* **21**, 054039 (2024).
291. Zhang, X., Zangeneh-Nejad, F., Chen, Z.-G., Lu, M.-H. & Christensen, J. A second wave of topological phenomena in photonics and acoustics. *Nature* **618**, 687–697 (2023).
292. Yang, Y. *et al.* Non-abelian physics in light and sound. *Science* **383**, eadf9621 (2024).
293. Galiffi, E. *et al.* Extreme light confinement and control in low-symmetry phonon-polaritonic crystals. *Nat. Rev. Mater.* **9**, 9–28 (2024).
294. Ueda, H. *et al.* Chiral phonons in quartz probed by x-rays. *Nature* **618**, 946–950 (2023).
295. Jiao, P., Mueller, J., Raney, J. R., Zheng, X. & Alavi, A. H. Mechanical metamaterials and beyond. *Nat. Commun.* **14**, 6004 (2023).
296. Bertoldi, K., Vitelli, V., Christensen, J. & Van Hecke, M. Flexible mechanical metamaterials. *Nat. Rev. Mater.* **2**, 1–11 (2017).
297. Van Mastrigt, R., Dijkstra, M., Van Hecke, M. & Coulais, C. Machine learning of implicit combinatorial rules in mechanical metamaterials. *Phys. Rev. Lett.* **129**, 198003 (2022).





**Box 2 | Temporal symmetries, energy conservation and reciprocity** The differential equations describing the classical dynamics of physical systems involve the time variable  $t$ , a continuous parameter related to the periodic dynamics of a clock on which all observers agree. These equations are generally invariant under the full time-reversal operation  $t \rightarrow -t$ , which corresponds to reversing the flow of time, watching the dynamics backward as in a movie played with a reversed sequence of images. The fact that the equations of physics are invariant under this operation means that the reversed movie is allowed by the laws of physics and could occur if one would start from the end with time-reversed initial conditions for all objects and particles, a property called microscopic reversibility. For a wave system, such full time reversal operation not only makes the wave go backward, but also reverts the motion of all particles inside and outside the medium, changing damping into amplification, and inverting the direction of moving objects, including spinning particles under the influence of an external field, or medium translations, rotations or time-dependency. The effective medium seen by the wave may therefore not be the same after time-reversal, with losses changed into gain and magnetic/kinetic effects reversed. Adopting the standpoint of the wave, we say that such media break time-reversal symmetry. Depending on whether the origin of this time-reversal symmetry breaking is due to non-conservation of energy, e.g., absorption, or the reversal of an external bias, such as magnetic or kinetic media, it has different consequences, as summarized for linear systems by the so-called Onsager microscopic reversibility equations<sup>111</sup>. In the case of non-conservative systems, the medium remains reciprocal, namely transmission coefficients are symmetric upon interchanging the locations of source and receiver. In the second case, reciprocity is violated. Nonlinear processes by themselves do not break time-reversal, but can break reciprocity<sup>110</sup>. A linear medium with a time-varying index of refraction may or may not break time-reversal symmetry, depending on how the time-dependency of the index changes when  $t \rightarrow -t$ , as shown in<sup>165</sup>. Finally, time-reversal symmetry is distinct from time-translation invariance  $t \rightarrow t - t_0$ , which makes the origin of time irrelevant and guarantees that the Hamiltonian is conserved. In turn, this implies that the total energy in the system is conserved, yet not necessarily the energy of the wave.

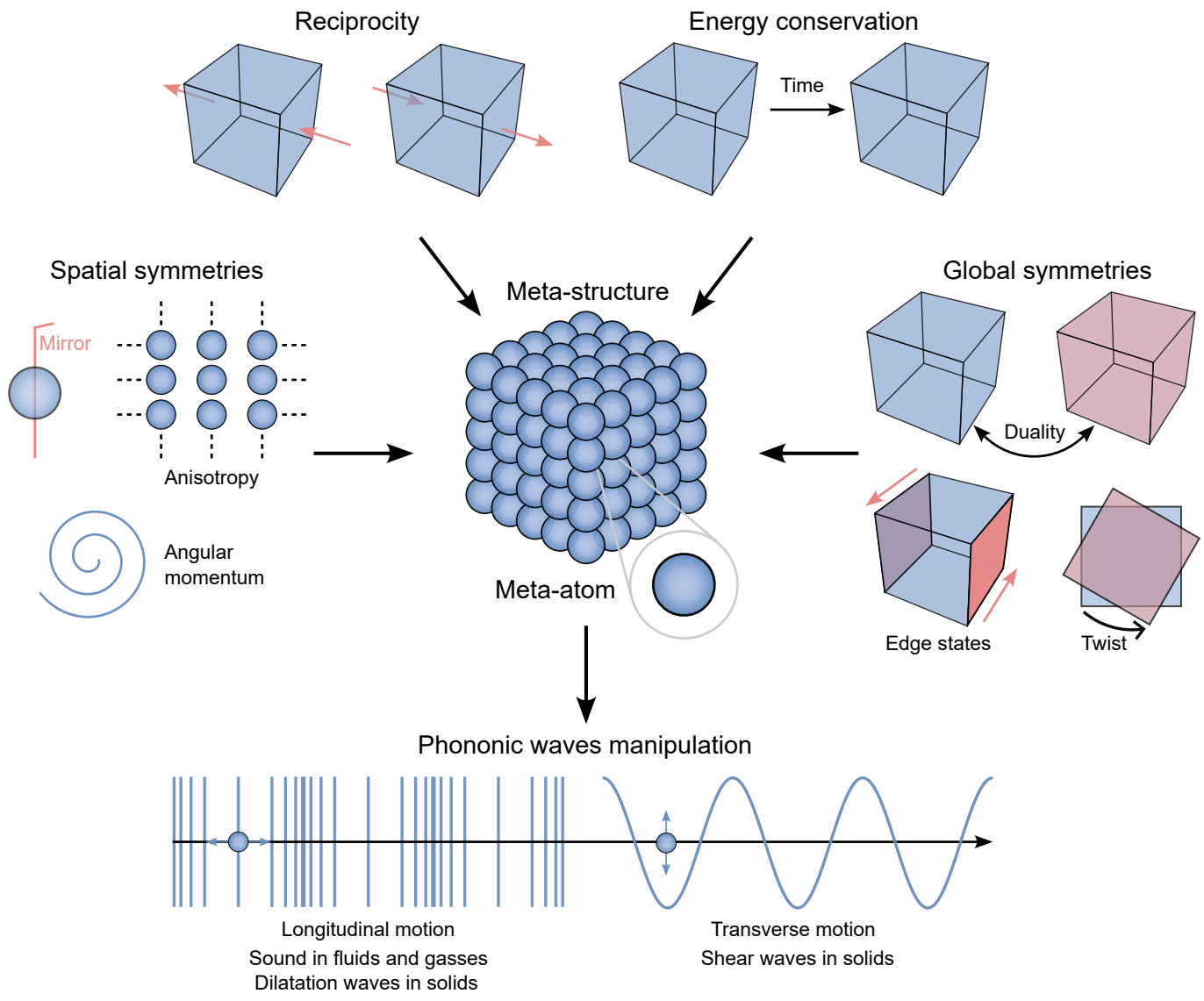


**Figure 1. Symmetry-driven phononics.** Identification and selective breaking of the various symmetries characterizing phononic materials and meta-structures, both at the microscopic and macroscopic scales. These broken symmetries enable enhanced control over acoustic and elastodynamic wave propagation. In this review we focus on different symmetry classes, namely spatial symmetries, reciprocity, energy conservation and global symmetries.

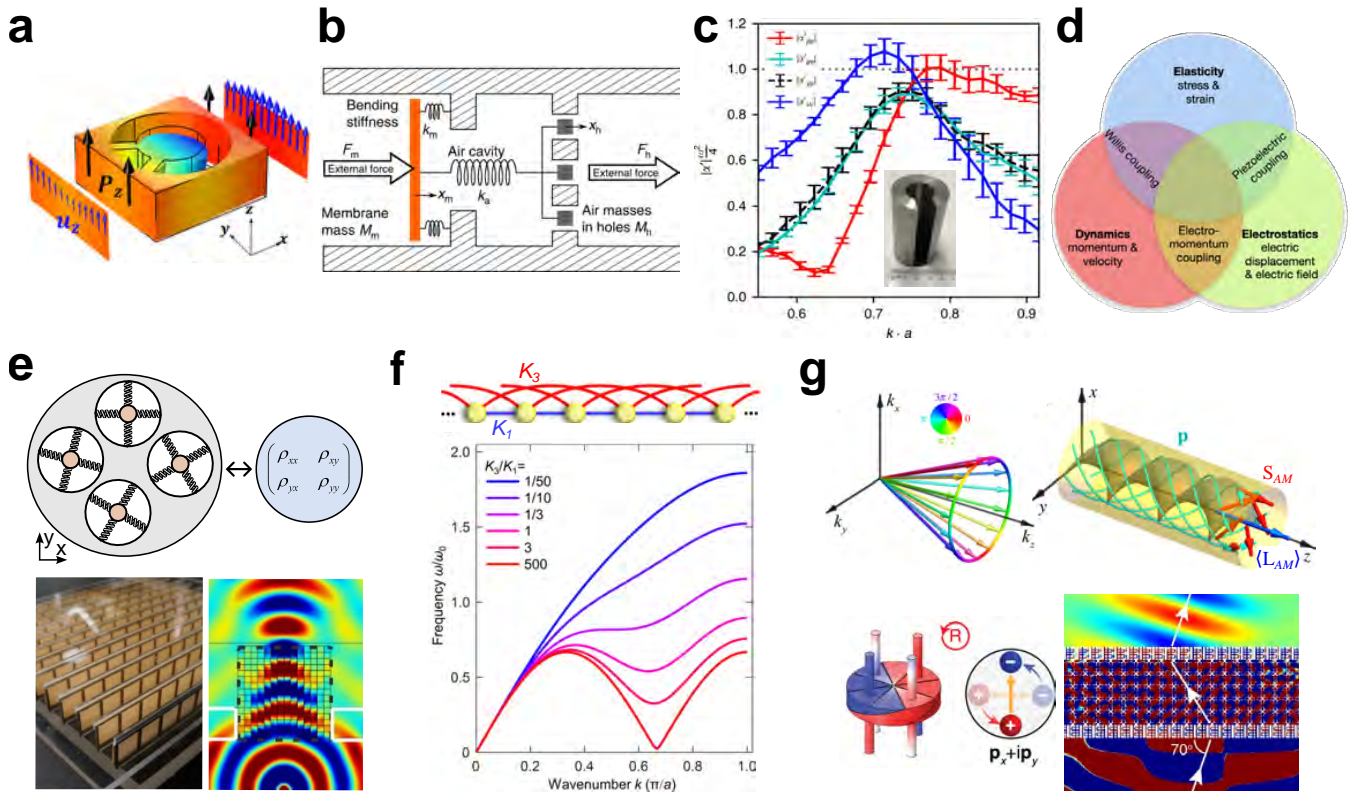


**Figure 2. Phononic phenomena controlled by spatial symmetries.** **a**, Willis coupling between momentum ( $P_z$ ) and strain  $\partial_x u_z$  stemming from a resonant meta-atom with broken spatial inversion symmetry, in the context of flexural waves in a structured beam. **b**, Experimental verification of the existence of Willis coupling for air-borne acoustic waves resulting from a scatterer with broken spatial inversion symmetry. **c**, Experimental verification of maximal off-diagonal polarizabilities within a Helmholtz resonator (inset) which match the conventional monopole and dipole polarizability (red and blue lines, respectively, in the right panel), and almost reach the theoretical bound fixed by passivity (gray dotted line in right panel). These off-diagonal polarizabilities result in maximal even acoustic Willis coupling. **d**, Diagram showing the multi-physics couplings that exist in a trianisotropic medium: Willis coupling, piezo-electricity and electro-momentum coupling. The local part of these interactions stems from different symmetry-breakings at the subwavelength scale. **e**, (Top) general model of an acoustic medium whose macroscopic effective response is modeled with a dynamic mass density tensor. (Bottom) acoustic metamaterial with membranes along one spatial direction (inset), leading to hyperbolic wavefronts propagation. **f**, Bending of the dispersion relation in a unidimensional chain of masses and springs as a function of the ratio between first-order and third order couplings. For a ratio equal to 1, the dispersion is analogous to that of a roton. **g**, (Top) Acoustic Bessel beam with a rotating phase profile (left) responsible for helicoidal wavefronts carrying non-zero integral orbital angular momentum  $\langle L_{AM} \rangle$  and spin angular momentum density  $\mathcal{S}_{AM}$  ( $\langle \mathcal{S}_{AM} \rangle = 0$  for a homogeneous field). (Bottom) Engineered twisted couplings in a metamaterial unit cell generate spin-orbit coupling for sound, which is harnessed to obtain negative refraction. Panel (a) reprinted with permission from<sup>17</sup>. American Physical Society. Panel (b) reprinted with permission from<sup>27</sup>. Springer Nature Limited. Panel (c) reprinted with permission from<sup>23</sup>. Springer Nature Limited. Panel (d) reprinted with permission from<sup>19</sup>. American Physical Society. Panel (e) (bottom) reprinted with permission from<sup>109</sup>. American Physical Society. Panel (f) reprinted with permission from<sup>71</sup>. Springer Nature Limited. Panel (g) (top) reprinted with permission from<sup>78</sup>. American Physical Society. (Bottom) reprinted with permission from<sup>102</sup>. Springer Nature Limited.

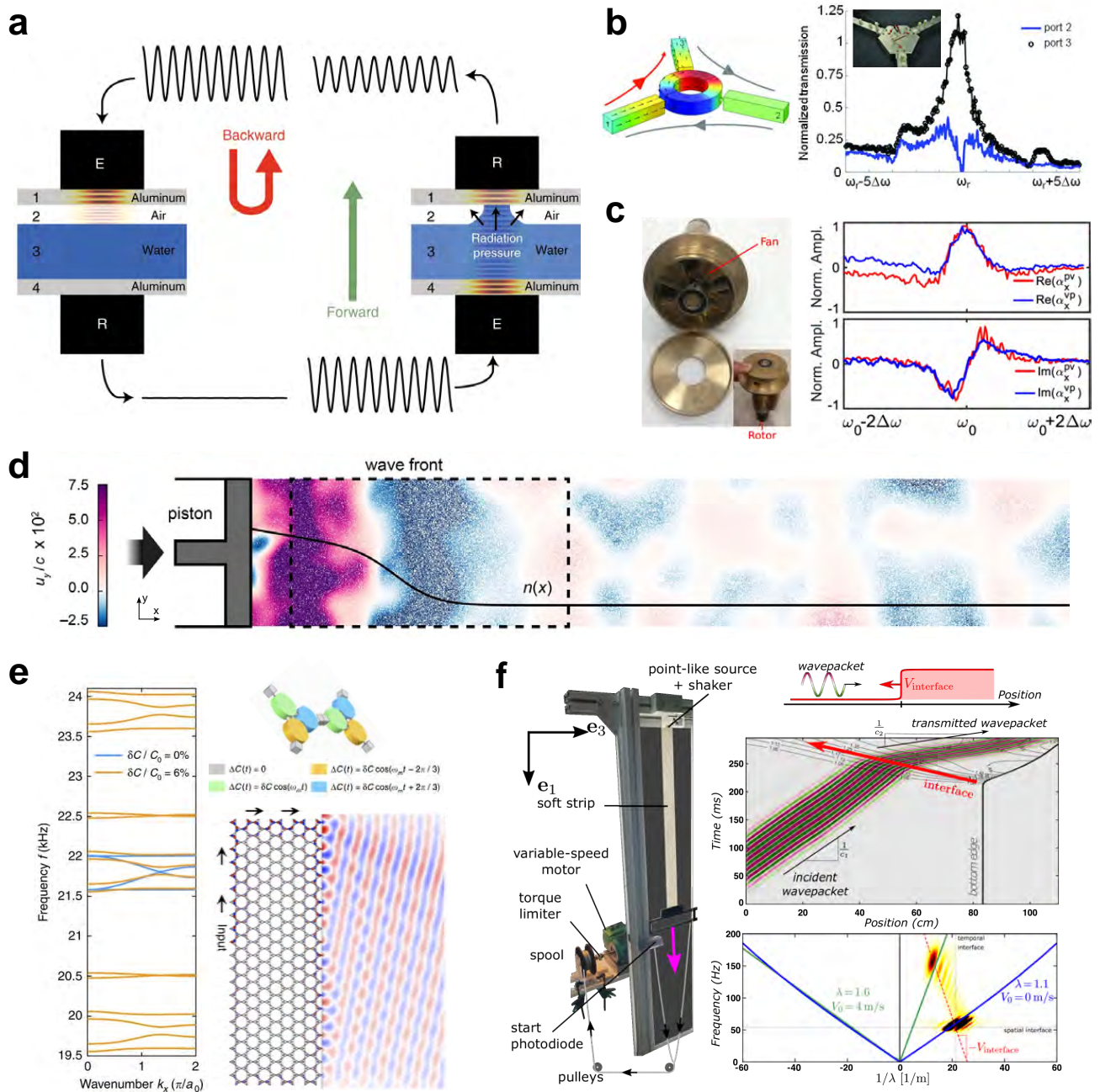


**Figure 3. Phononic phenomena controlled by time-symmetry and reciprocity.** **a**, Non-reciprocal phonon transmission induced by the combination of spatial asymmetry and nonlinearity stemming from the acoustic radiation pressure at the interface between air and water. **b**, Acoustic circulator based on a three-port cavity (left panel) with embedded flow leads zero transmission from port 1 to 2, and full transmission from port 1 to 3, at the resonance frequency (right panel). **c**, Experimental measurement of acoustic polarizations corresponding to odd Willis coupling (right panel) induced by time-reversal symmetry breaking within a biased, spatially symmetrical scatterer (left panel). Here, the bias consists of an asymmetric flow, obtained with a motorized fan. **d**, A shock wave propagating in a chiral active fluid with odd viscosity yields a directional transverse flow. **e**, Band structure of a Floquet topological insulator for sound (left panel) based on unit cells with a periodic time-modulation with a directional angular phase profile (top right panel), resulting in a topologically protected, non-reciprocal acoustic leaky-wave antenna (bottom right panel). **f**, Flexural wave packets crossing a spatio-temporal interface upon the abrupt deformation of a soft elastomer. This results in the non-conservation of both wavenumber and frequency, thereby leading to different behavior depending on the excitation direction. Panel (a) reprinted with permission from<sup>118</sup>. Springer Nature Limited. Panel (b) reprinted with permission from<sup>129</sup>. American Association for the Advancement of Science. Panel (c) reprinted with permission from<sup>135</sup>. Springer Nature Limited. Panel (d) reprinted with permission from<sup>149</sup>. Springer Nature Limited. Panel (e) reprinted with permission from<sup>158</sup>. Springer Nature Limited. Panel (f) reprinted with permission from<sup>185</sup>. arxiv.

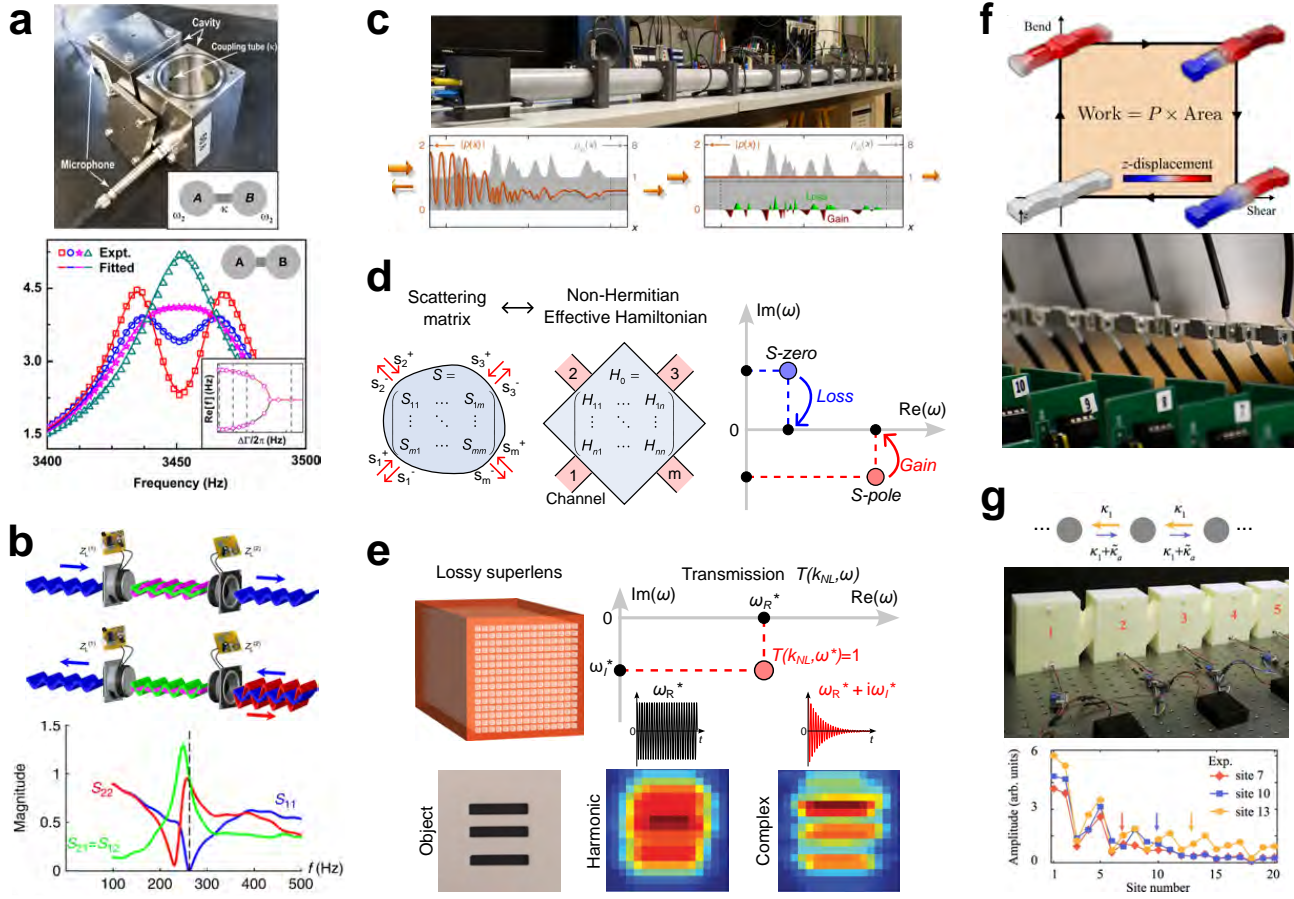


**Figure 4. Phononic phenomena controlled by time symmetry and energy conservation.** **a**, A two-level non-Hermitian system made of two tightly-coupled acoustic cavities with controllable asymmetric loss (top panel) which allows to demonstrate the coalescence of the two modes at the exceptional point, evidenced by the merging of the two transmission peaks depending on the loss amount (bottom panel). **b**, An invisible acoustic sensor based on  $\mathcal{PT}$ -symmetry, showcasing unitary transmission ( $S_{12} = S_{21} = 1$ ) which is reflection-less from one side ( $S_{11} = 0$ ), and with strong reflection from the other side (bottom panel, at gray dotted line frequency). Here, gain and loss are obtained with impedance circuit design. **c**, (Bottom left panel) In a disordered Hermitian acoustic system, part of the incident signal is reflected due to spatial variations of the medium properties (gray area). (Bottom right panel) a tailored gain-loss distribution permits to obtain a perfect transmission through the sample, along with no pressure variations within the system. (Top panel) this non-Hermitian design has been implemented discretely using electrodynamic loudspeakers with a controlled acoustic impedance. **d**, (Left panel) Correspondence between the scattering matrix  $S$  of a system with  $m$  ports and an effective Hamiltonian, obtained from the original  $n \times n$  Hermitian Hamiltonian  $H_0$  with additional non-Hermitian corrections associated with the coupling to  $m$  channels. (Right panel) representing the corresponding scattering matrix in the complex frequency plane shows poles and zeros which can be moved to the real frequency axis using loss and gain. **e**, The resolution of a conventional acoustic superlens is limited by its nonlocality,  $k_{NL}$  being the associated largest wavenumber accessible, and by inherent dissipation which pushes the corresponding unitary transmission  $T(k_{NL}, \omega^*) = 1$  below the real frequency axis. Using the associated complex excitation ( $\omega^* = \omega_R^* + i\omega_I^*$ ), whose imaginary part is related to the losses of the system, instead of the monochromatic signal ( $\omega_R^*$ ), results in a virtual gain that effectively compensate the losses in the lens and leads to enhanced resolution. **f**, It is possible to induce odd properties to the elastic features of a mechanical beam using electrically controlled piezoelectric patches (bottom panel). In such a medium, a quasistatic cycle between bending and shear motion of the unit cell is associated with a non-zero work per unit volume (top panel). **g**, Non-Hermitian skin effect in a chain of active acoustic resonators based on asymmetric couplings, which are here implemented using active feedback loops between speakers and microphones. Panel (a) reprinted with permission from<sup>191</sup>. American Physical Society. Panel (b) reprinted with permission from<sup>201</sup>. Springer Nature Limited. Panel (c) reprinted with permission from<sup>202</sup>. Springer Nature Limited. Panel (e) reprinted with permission from<sup>216</sup>. American Physical Society. Panel (f) reprinted with permission from<sup>219</sup>. Springer Nature Limited. Panel (g) reprinted with permission from<sup>228</sup>. Springer Nature Limited.

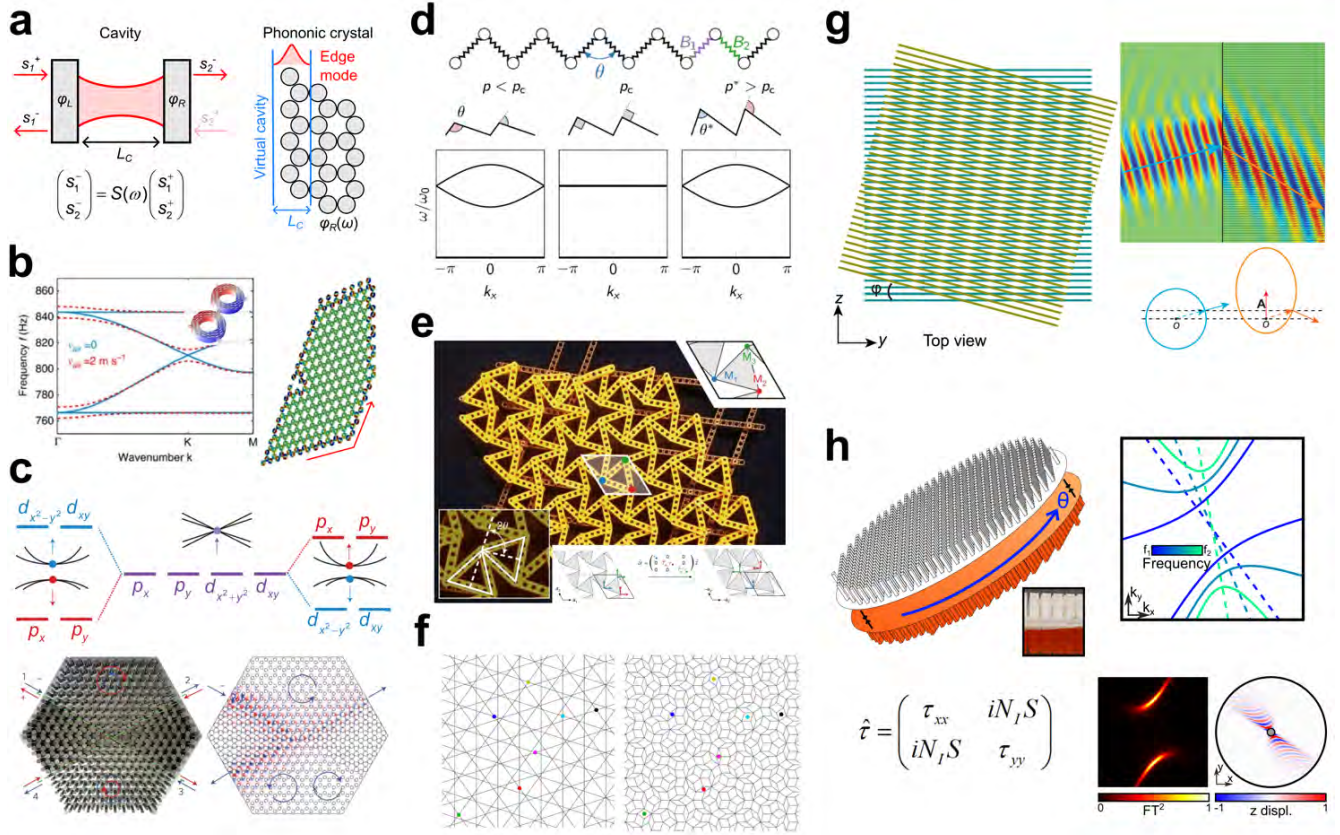


**Figure 5. Phononic phenomena controlled by global symmetries.** **a**, Correspondence between a conventional resonant cavity made of two mirrors with reflection phases  $\phi_{L,R}$ , described by a scattering matrix  $S(\omega)$  (left panel) and the virtual cavity at the edge of a gapped phononic crystal, whose reflection phase  $\phi_R(\omega)$  depends on the operating frequency, hosting a boundary mode. **b**, Flow-induced time-reversal symmetry breaking in an acoustic honeycomb lattice lifts the Dirac cone degeneracy and open a topological bandgap described by a Chern invariant. Such a phononic Chern insulator exhibits topologically protected non-reciprocal wave propagation at its boundaries. **c**, The preservation of  $C_{6v}$  spatial-symmetry within triangular lattices of pillars, as well as the symmetrical band inversion induced by changing the pillars' radius, results in helicoidal topological boundary states whose symmetry-engineered pseudo-spin allows for wave sorting at topological crossings. **d**, Three different configurations of a mass-spring chain show the emergence of a hidden symmetry, or duality, that results in two different lattices with the same band structure (left and right panels). At the self-dual point (center panel), the duality becomes a symmetry of the medium, and leads to a double degeneracy of the band for the entire Brillouin zone. **e**, In the plane, twisted Kagome lattice also host a duality that relates the orientation of the masses degree-of-freedom with respect to the lattice (bottom right inset). **f**, Duality between quasi-crystals and fiber networks, with a few highlighted nodes of the network and their dual parallelograms (color dots). **g**, The twist between phononic crystal layers (left panel) induces a gauge field leading to negative refraction of acoustic waves (top right panel), described by a shift of the isofrequency contours in the reciprocal space (bottom right panel). **h**, The twist between two detuned anisotropic elastic metasurfaces (left) leads to a frequency dependency of the bilayer's hyperbolic contour orientation (top right panel). This axial dispersion comes with an asymmetric distribution of losses, which results in shear hyperbolic wavefronts (bottom right panel). Panel (b) reprinted with permission from<sup>130</sup>. Springer Nature Limited. Panel (c) reprinted with permission from<sup>258</sup>. Springer Nature Limited. Panel (d) reprinted with permission from<sup>263</sup>. American Physical Society. Panel (e) reprinted with permission from<sup>262</sup>. Springer Nature Limited. Panel (f) reprinted with permission from<sup>266</sup>. American Physical Society. Panel (g) reprinted with permission from<sup>283</sup>. American Association for the Advancement of Science. Panel (h) reprinted with permission from<sup>287</sup>. American Physical Society.